International Journal of Engineering Science 208 (2025) 104194

Contents lists available at ScienceDirect

International Journal of Engineering Science

journal homepage: www.elsevier.com/locate/ijengsci

Full length article

Exploring the impact of thermal fluctuations on continuous models of adhesion

Claudia Binetti [a,b], Andrea Cannizzo [a,b], Giuseppe Florio [b,c], Nicola M. Pugno [d,e], Giuseppe Puglisi [b,*], Stefano Giordano [a]

[a] University of Lille, CNRS, Centrale Lille, Univ. Polytechnique Hauts-de-France, UMR 8520 - IEMN - Institute of Electronics, Microelectronics and Nanotechnology, F-59000 Lille, France
[b] Department of Civil Environmental Land Building Engineering and Chemistry, DICATECh, Polytechnic University of Bari, via Orabona 4, 70125 Bari, Italy
[c] INFN, Section of Bari, I-70126, Italy
[d] Laboratory for Bioinspired, Bionic, Nano, Meta Materials & Mechanics, University of Trento, Via Mesiano 77, 38123 Trento, Italy
[e] School of Engineering and Materials Science, Queen Mary University of London, Mile End Road, London E1 4NS, UK

ARTICLE INFO

Keywords:
Adhesion
Thermal effects
Griffith approach
Phase Transition
Multiscale models
Statistical Mechanics

ABSTRACT

Adhesion and deadhesion processes at the interface between an object and a substrate are well-established phenomena in the realm of materials science and biophysics. These processes can be profoundly influenced by thermal fluctuations, a phenomenon empirically validated through numerous experimental observations. While discrete models have traditionally served as a foundation for understanding this intricate interplay, this paper seeks to bridge the gap between such discrete representations and the continuous models that more accurately reflect experimental scenarios. To achieve this objective, we initially adopt discrete models comprising n elements, selected such that their physical parameters converge towards the continuum limit as n approaches infinity. This thoughtful scaling ensures that the discrete system retains its relevance in the context of continuous media. Leveraging principles from Statistical Mechanics and Griffith-type total energy minimization approaches, we employ this scaled discrete model to investigate the impact of temperature in continuous adhesion phenomena. As a result, we obtain an analytical model to account for the decrease of the decohesion threshold depending on thermal (entropic) energy terms. Interestingly, our approach demonstrates that continuous adhesion models invariably exhibit phase transitions, whose critical temperatures can be derived through closed-form calculations. By elucidating these critical temperature values, this work enhances our understanding of adhesion processes within continuous media and opens new avenues for the exploration of adhesion-related phenomena in diverse scientific disciplines. Finally, the comparison with some experimental results is discussed.

1. Introduction

Adhesion and deadhesion phenomena are ubiquitous across a spectrum of physical, biological, and technological systems, as highlighted by previous research studies (Dillard & Pocius, 2002; Israelachvili, 2011; Kendall, 2004). These phenomena manifest through a diverse range of mechanisms, spanning from molecular interactions at the nanoscale to mechanical forces at the

* Corresponding author.
E-mail addresses: claudia.binetti@iemn.fr (C. Binetti), andreacannizzo1992@gmail.com (A. Cannizzo), giuseppe.florio@poliba.it (G. Florio), nicola.pugno@unitn.it (N.M. Pugno), giuseppe.puglisi@poliba.it (G. Puglisi), stefano.giordano@univ-lille.fr (S. Giordano).

https://doi.org/10.1016/j.ijengsci.2024.104194
Received 14 March 2024; Received in revised form 9 December 2024; Accepted 12 December 2024
Available online 24 December 2024

mesoscale (Kendall, 1994). Their far-reaching implications extend to various domains, including, but not limited to, the industrial sectors (automotive, aerospace, biomedical, and microelectronics) (Baldan, 2012; Haisma & Spierings, 2002), the intricate interplay of contact and adhesion in soft materials (Creton & Ciccotti, 2016; Shull, 2002), adhesion phenomena in polymer films (Barreau et al., 2017; Gong et al., 2019; Kwak et al., 2018), bonding of dental materials (Eick et al., 1997; Marshall et al., 2010), and the critical role of adhesion in cells interaction and motility (Fuhrmann & Engler, 2015; Khalili & Ahmad, 2015; Rico et al., 2010; Ron et al., 2020).

One commonality among adhesion processes is their susceptibility to thermal fluctuations, as supported by numerous experimental findings (Adams et al., 1992; Kim et al., 2020; Lai et al., 2015; Niewiarowski et al., 2008). This effect is particularly pronounced in nanomaterials and nanostructures, where thermal energy can rival mechanical energy, facilitating spontaneous deadhesion (Gojzewski et al., 2017; Zilberman & Persson, 2003). Indeed, in most cases, the force needed to separate a film from its substrate diminishes with rising temperature. This reduction in adhesion strength can be attributed, in several important cases, to thermal fluctuations, which facilitate the exploration of phase space. One may think in particular to low (nanometers) scales systems (Merkel et al., 1999; Tang et al., 2006), or larger systems constituted by macromolecules whose elasticity is of the entropic type, such as protein and rubber-like materials (Treloar, 1975). Likewise, the diffusely observed rate dependence in the decohesion mechanisms can be referred to thermal fluctuations and the consequent activation processes (Chaudhury, 1999). As a result, even when external forces alone would not lead to detachment, thermal fluctuations can drive the system into phase space regions where rupture occurs. Sometimes, as an extreme example highlighting the significance of the described thermal effects, the force required for deadhesion diminishes to zero for large temperature values, indicating a phase transition characterized by a specific critical temperature. Beyond this critical temperature, the system consistently remains in a debonded state, regardless of the applied mechanical conditions. This behavior has been shown for several systems where adhesion and cohesion phenomena occur. Concerning cell adhesion, it has been experimentally observed that the attachment strength monotonically decreases with increasing temperature, regardless of substrate properties (Fuhrmann & Engler, 2015; Rico et al., 2010), and a possible phase transition can be inferred from experimental data (Fuhrmann & Engler, 2015). It is worth noting that the physics of cell adhesion, particularly its critical behavior, has received extensive theoretical scrutiny (Blom & Godec, 2021; Schwarz & Safran, 2013). Moreover, researchers have conducted experimental investigations into the mechanical unfolding of nucleic acid hairpins, aiming to establish a phase diagram within the force-temperature plane. For both RNA and DNA, it has been observed that the force required to separate the two polynucleotide strands decreases as temperature rises, exhibiting indications of a phase transition at a critical temperature known as the denaturation temperature (De Lorenzo et al., 2015; Stephenson et al., 2014). These findings have received additional support from several numerical and theoretical investigations, which confirm the presence of this critical behavior in nucleic acids (Florio & Puglisi, 2023; Hyeon & Thirumalai, 2005; Mishra et al., 2011; Peyrard, 2004; Peyrard & Bishop, 1989). In materials science, similar phenomena have also been observed. A historical example can be found in the study of sapphire whisker fractures at various temperatures (Brenner, 1962). Once again, there is a discernible trend of decreasing fracture strength with increasing temperature, culminating in a well-defined phase transition at elevated temperatures (Brenner, 1962). It is important to note that while fracture and adhesion represent distinct phenomena, they exhibit noteworthy similarities in small systems. The reconciliation of these two effects is rooted in the Lake and Thomas effect, which demonstrates that the effective fracture energy, significantly larger than the breaking energy of single bonds belonging to the fracture surface, is measured by the simultaneous stretching and breaking of bonds at the interface. This behavior closely resembles the phenomena underlying decohesion between polymeric layers (Ghatak et al., 2000; Lake & Thomas, 1967). More recent studies have further validated these observations, extending their validity to materials engineered to withstand high-temperature environments (Bayer & Cooper, 1969; Shao et al., 2019), including high-entropy and medium-entropy alloys (Miracle & Senkov, 2017). On the other hand, we remark that many other effects influencing adhesion properties can be associated to temperature changes such as glass transition in polymers adhesion (Cassidy et al., 1972), capillarity effects (Lai et al., 2015), temperature dependent moduli (Barker, 1963), or chemical effects (Awada et al., 2011).

Given the significant impact of thermal fluctuations on adhesion phenomena, theoretical models are essential for explaining and predicting the behaviors described above (Ciavarella et al., 2019; Dasanna et al., 2020; DiMilla et al., 1991; Johnson, 1998; Maddalena et al., 2009; Puglisi & Truskinovsky, 2013). The method of spin variables has proven valuable in studying thermal effects in systems with non-convex energies (Bellino et al., 2020; Benedito & Giordano, 2018a, 2018b; Cannizzo et al., 2022; Cannizzo & Giordano, 2023; Florio & Puglisi, 2019; Giordano, 2017, 2022, 2023), in particular for adhesion phenomena (Cannizzo et al., 2021; Florio et al., 2020). In this context, it became possible to demonstrate the existence of critical phenomena in systems characterized by a discrete set of bonds, which can either remain intact or broken (Florio et al., 2020). Furthermore, this concept extends to systems where the bonds can undergo damage (softening), before the complete debonding (Cannizzo et al., 2021). This framework is capable of describing dissipative phenomena and cohesive fracture effects. In these methodologies, the introduction of domain walls between intact, softened and broken regions simplifies the mathematical analysis (Cannizzo et al., 2021; Florio et al., 2020). At the same time, various models have been proposed to investigate the influence of temperature on membrane adhesion using more arbitrary discrete distributions of bonds. These models encompass two-dimensional lattice gas and Coulomb plasma models (Speck et al., 2010; Zuckerman & Bruinsma, 1995). The same approaches have been generalized to explore the dynamic behavior of adhesion processes as well (Bihr et al., 2012; Reister-Gottfried et al., 2008). Furthermore, experimental and theoretical methods have been used to study thermal effects on van der Waals adhesive forces (Pinon et al., 2016), and Monte Carlo simulations have been performed to analyze the temperature dependence of vesicle adhesion (Gruhn & Lipowsky, 2005).

While all these models do consider temperature, they are essentially discrete and often lack analytical solutions, thereby limiting the clarity of the obtained results. In this paper, our aim is to introduce a methodology for studying the Statistical Mechanics of adhesion, but with the crucial objective of deducing continuous limit models with explicit analytical results. Indeed, it is important

to emphasize that the literature lacks continuous models of adhesion phenomena that rigorously incorporate thermal effects based on Statistical Mechanics. Continuous models are essential for describing biological systems or artificial systems in engineering and nanotechnology that are sufficiently large, making a detailed molecular-level study impractical. Furthermore, continuous models are crucial for adapting and coupling these descriptions with the classical mechanics of materials. The originality of the approach lies in the concurrent introduction of both the discrete model (so to apply the methods of Statistical Mechanics) and the corresponding continuous model (the approach of Continuum Mechanics). Our theory is inspired by the approaches proposed by Bellino et al. (2023) and Di Stefano et al. (2022), where discrete and continuum limits for the fibrillar adhesion of shear loaded systems are discussed, with application in focal adhesion. The extension to thermal and rate effects of this system has been developed by Bellino (2022).

To this end, we start with the definition of a discrete model composed of n elements, with the physical parameters which suitably rescale towards a continuous model for $n \to \infty$. Firstly, we conduct an analysis of the system for the purely mechanical case without considering thermal fluctuations. Then, in a second step, we incorporate the effects of Statistical Mechanics to describe fluctuations and the resulting temperature effects. In the first analysis, we initially consider the energy of the discrete system, and we successively perform the limit for $n \to \infty$, eventually obtaining this quantity in integral form. We refer to the relevant literature for the rigorous (Γ-convergence) framework of the problem (Braides, 2002; Maddalena et al., 2009; Maso, 1993; Puglisi & Truskinovsky, 2013), whereas the detailed thermodynamic problem and a reconciliation of micro- and macro-properties have been studied by Puglisi and Truskinovky (2005).

Following the Lake and Thomas extension (Ghatak et al., 2000; Lake & Thomas, 1967), generalizing the Griffith criterion of fracture (Griffith, 1921; Pugno, 2021), the total energy is composed of the elastic energy of the deformable film and the rupture energy corresponding to the detached region of the system. This represents an important extension of the Griffith hypothesis because the energy required for the decohesion front propagation measures the total energy needed to extend the molecules up to the unbonding. This includes the energy associated with the significant stretching of neighboring molecular chains. We assume a linear behavior here, but this can be extended to nonlinear cases as well. As expected, the debonding energy depends on the total elongation energy up to fracture and on the stiffness of the attached layer: a higher stiffness leads to a larger number of stretched chains and, thus, to a larger debonding energy. This allows us to overcome the known underestimation of the Griffith hypothesis, where the debonding energy measures only the energy for the bond breaking. While the proposed scheme is merely prototypical of full two-dimensional systems, it enables a complete analytical description, addressing both the entropic energy terms and the resulting temperature dependence of the fracture phenomenon. It is important to note that alternative strategies to the Griffith hypothesis exist to represent the effect of the driving force acting on the decohesion propagating front. Indeed, analyzing the local and global stability of all solutions can lead to different transition strategies.

Based on the proposed model, we first apply a Griffith's type criterion to the adhesion problem and determine the minimum threshold of applied mechanical action sufficient to detach the film from the substrate when thermal effects are neglected (purely mechanical limit). Based on the discreteness of the proposed prototypical model, we are then able to inscribe our model in the framework of classical Statistical Mechanics. Indeed, the discrete structure of our model allows for the definition and calculation of the partition function of the system, and the corresponding Gibbs or Helmholtz free energy. In this case, the limit for $n \to \infty$ is applied after the explicit calculation of the partition function, and so the free energies refer to a continuous system. The formal derivation of this limit can be deduced based on the classical $\Gamma-$convergence theory (Braides, 2002; Maso, 1993), whereas the continuum limit of the equilibrium configurations requires the application of classical linear algebra theorems on tridiagonal matrices (Usmani, 1994a, 1994b). In the purely mechanical setting of adhesion such an approach has been previously adopted in the description of the hierarchical mechanics of gecko's adhesion (Maddalena et al., 2009; Puglisi & Truskinovsky, 2013).

It is important to remark that the continuum limit can be performed in two different ways. A first approach consists in considering a fixed Boltzmann constant and an increasing density of the particles in a fixed length L (*i.e.*, $L = n\ell$ constant, with $n \to \infty$ and $\ell \to 0$). This procedure is typically used in statistical field theory and is able to preserve the trace of the underlying discrete structure (Parisi, 1988). It means that it allows the preservation of any phase transitions observed in the corresponding discrete models (Itzykson & Drouffe, 1989a, 1989b). However, an infinite number of particles studied with a fixed Boltzmann constant clearly induces an infinite entropy and thus a complete and consistent thermodynamic construction is lost. A second possibility considers a Boltzmann constant rescaled with the number of particles n, *i.e.* $k_B \sim 1/n$, when $n \to \infty$ (Bruin & Compagner, 1973; Compagner, 1989). This assumption must be coupled with a Planck constant rescaled as $h \sim 1/n^2$, as fully explained by Compagner (1989). In this case, the effect of thermal fluctuations is reduced in order to maintain a finite entropy. This procedure generates therefore a coherent set of thermodynamic relations, but disrupts the possible phase transitions. Of course, the choice between these two different approaches to the continuum limit must be made according to the physical reality one wishes to describe. In our case, we know that discrete adhesion models involve phase transitions (Cannizzo et al., 2021; Florio et al., 2020), so we choose the approach described by a fixed Boltzmann constant.

The fundamental important novelty of the model here proposed is that now Griffith's propagation criterion is applied by replacing the mechanical energy with the thermodynamic free energy (Stevens & Guiu, 1991). In this regards, again in accordance with the Griffith approach, both the partition functions and the free energies are determined at fixed fraction of the detached zone in order to study the detachment criterion for the given configuration. Hence, this fraction is considered here as a Landau order parameter of the process, thus assuming that the characteristic time of the decohesion mechanism is much larger than the thermalization time of all microstates (Goldenfeld, 2018; Huang, 1987). This represents a fundamental difference with respect to previous works of some of the authors of the present paper (Cannizzo et al., 2021; Florio et al., 2020). Indeed, in the present framework of Griffith-type energy minimization, the energy is not minimized with respect to the debonding fraction; instead, the debonding fraction evolves

according to the driving force. This is the exact application of Griffith's criterion, as opposed to the global energy minimization approach proposed, *e.g.*, by Francfort and Marigo (1998). On the other hand, we note that, unlike Griffith's classical approach which requires the existence of a pre-existing detached region, our model also allows us to determine an analytical expression for the decohesion nucleation threshold.

Based on this principle we obtain that the purely mechanical detachment threshold, previously discussed, must be multiplied by a factor $\sqrt{1-T/T_c}$, when there are thermal fluctuations at temperature T. As a result, the described continuous adhesion processes are characterized by a second order phase transition with critical temperature T_c, the value of which, depending on the macroscale molecular properties of the material, has been explicitly calculated. This analysis was developed in the load-controlled Gibbs statistical ensemble, which corresponds to the application of a force to detach the film, and in the displacement-controlled Helmholtz statistical ensemble characterized by the prescription of the position of the end of the film itself (Manca et al., 2012). From the experimental point of view, we remark that the load-controlled Gibbs ensemble and the displacement-controlled Helmholtz ensembles correspond, respectively, to boundary conditions obtained by controlling the force applied with soft devices or the position imposed with hard devices to the end of the peeling film (Bellino et al., 2019). We pointed out similarities and differences between the two statistical ensembles, making it easier to apply them to real cases from materials science and biophysics. In particular, we show the different behavior in term of the existence of stable propagation fronts (Zehnder, 2012). While the detachment propagation is always unstable in the case of assigned force, independently on temperature, in the case of assigned displacement the propagation can be stable (coherent quasi-static propagation) depending on the initial detachment extension and the temperature.

The obtained results can be implemented to better understand adhesion mechanisms in cell biophysics, soft matter, healthcare materials, and micro- and nano-technology. As an example, the final part of the paper is devoted to the analysis of the temperature dependent decohesion behavior in a classical double-cantilever beam experiment on a carbon-epoxy laminates bonded with a ductile epoxy adhesive (Fernandes et al., 2016). The example exhibits the ability of the proposed model of catching the main energy competition terms for real systems in decohesion phenomena when thermal effects play an important role.

The paper is structured as follows. In Section 2, we study the load-controlled Gibbs ensemble, and in Section 3 the displacement-controlled Helmholtz ensemble. In both cases, we firstly examine the purely mechanical behavior of the adhesion processes and then we introduce the framework of Statistical Mechanics to study the corresponding phase transitions. For the Helmholtz ensemble, we also discuss a comparison with recent experimental results. Conclusions and two mathematical appendices close the article.

2. Load-controlled Gibbs ensemble: soft device

In this section, we develop the theory of adhesion and deadhesion for a film deposited on a substrate and detached by applying a force to one of the specimen ends (see Fig. 1). Drawing an analogy from the statistical constant-pressure ensemble employed in Statistical Mechanics, we refer to this configuration as a Gibbs ensemble. From an experimental perspective, this configuration can be realized using soft devices, characterized by an intrinsic elastic stiffness much lower than that of the film under tension. We begin by analyzing the purely mechanical deadhesion process employing the calculus of variations and the Griffith energy criterion. Following this, we explore the impact of thermal fluctuations through the lens of Statistical Mechanics. Notably, we assume that the propagation criterion remains applicable, with the mechanical energy being replaced by the Gibbs free energy.

This statistical ensemble stands in dual contrast to the one defined by specifying the position of the film's right-end terminal. We will delve into this second statistical configuration, referred to as the Helmholtz ensemble, in a subsequent section.

2.1. Purely mechanical deadhesion

We start by introducing the discrete structure of the model, taking care to define the values of the physical parameters so that they scale correctly to lead to the continuum limit. We consider n vertical springs with elastic constant k_t that can be intact, with spin variable $\chi_i = 0$, or broken, with spin variable $\chi_i = 1$. The spin variable is in fact a binary variable introduced to discriminate the intact or broken state of each vertical element. We remark that the broken state is associated to an additional energy, corresponding to the amount of energy required to break the element. On the one hand, each intact vertical element is described by an energy $\frac{1}{2}k_t y_i^2$, where y_i is its extension. On the other hand, a broken element is associated with the energy $\frac{1}{2}k_t y_m^2$, where y_m is a constant representing the extension at which the element breaks. In this manner, we maintain coherence with the Lake and Thomas approach (Ghatak et al., 2000; Lake & Thomas, 1967), which incorporates in the debonding energy the entirety of the energy required for the molecule to break, as well as the energy of the neighboring molecules involved in the decohesion phenomenon.

The film is then described by $n-1$ horizontal unbreakable springs with elastic constant k_ℓ, see Fig. 1*a*. To further simplify the analysis, we consider shear springs in our model (Maddalena et al., 2009; Puglisi & Truskinovsky, 2013). We remark that, as well known, a fully consistent theory cannot consider only shear effects without considering bending effects. On the other hand, in the special case of very thick beams, shear effects can be predominant. Since in the case of the adhesion process the adhesive is stretched by applying a load to one end and fixed on the opposite side, the pure shear assumption can be considered particularly relevant. However, we point out that in the discrete case, bending effects could be incorporated by introducing a potential energy term based on three points instead of two, as used in our current model. Consequently, the corresponding matrix would become pentadiagonal rather than tridiagonal, see for instance Eqs. (35) and (84) (Buche & Grutzik, 2024). Similarly, the order of the differential equation derived in the following in the continuous model would increase. This is outside the scope of the present approach, which focuses on achieving as much physical understanding as possible while avoiding any analytical complications. Some generalizations in this perspective are briefly outlined in the closing Section 4.

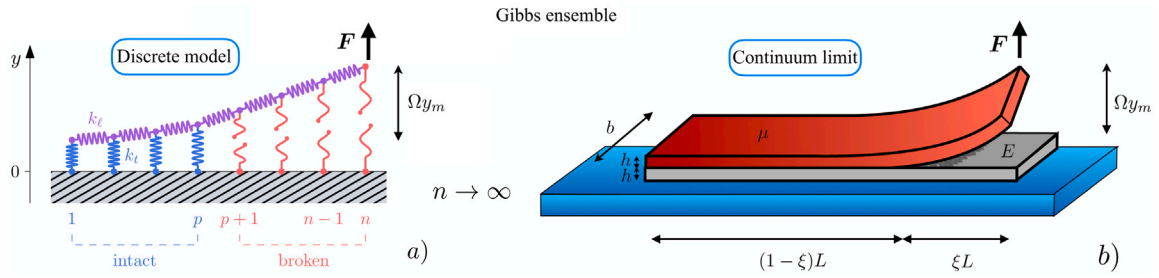

Fig. 1. Scheme of the adhesion model. (*a*): discrete structure of the model with horizontal and vertical springs, having elastic constants k_ℓ and k_t, respectively. The vertical springs break when $y_i = y_m$, $\forall i = 1, \dots, n$. We imposed $\chi_i = 0$ for $1 \le i \le p$, and $\chi_i = 1$ for $p+1 \le i \le n$ (see the main text for details). (*b*): continuous structure of the deposited film with Young's modulus E and shear modulus μ (L is the total length of the film, b is its depth, and h its thickness). The applied force F and the resulting extension Ωy_m are also displayed.

The Gibbs ensemble is characterized by a force F, here applied to the right end terminal of the system. By neglecting inertial terms, we can therefore write the total mechanical energy of the system (internal energy plus the potential energy of the applied force) as

$$\Phi_G = \frac{1}{2}\sum_{i=1}^{n}(1-\chi_i)k_t y_i^2 + \frac{1}{2}\sum_{i=1}^{n}\chi_i k_t y_m^2 + \frac{1}{2}\sum_{i=1}^{n-1}k_\ell (y_{i+1}-y_i)^2 - F y_n. \tag{1}$$

The phase space of the system is described by the vector $\boldsymbol{y} = (y_1, y_2, \dots, y_n) \in \mathbb{R}^n$. In order to have a correct continuum limit behavior, we assign the material parameters as follows

$$k_t = \frac{ELb}{nh}, \tag{2}$$

$$k_\ell = \frac{n\mu h b}{L}, \tag{3}$$

where E is the Young's modulus, μ is the shear modulus, L is the total length of the system, b is its depth, and h its thickness, see Fig. 1*b*. Then, we can obtain a dimensionless version $\tilde{\Phi}_G$ of the energy Φ_G by dividing Eq. (1) by

$$G^f = \frac{ELby_m^2}{h}, \tag{4}$$

representing the fracture energy of the fully detached beam. The result is

$$\tilde{\Phi}_G = \frac{\Phi_G}{G^f} = \frac{1}{n}\sum_{i=1}^{n}\frac{1}{2}(1-\chi_i)\omega_i^2 + \frac{1}{n}\sum_{i=1}^{n}\frac{1}{2}\chi_i + \frac{1}{n}\sum_{i=1}^{n-1}\frac{n^2h^2\mu}{2L^2E}(\omega_{i+1}-\omega_i)^2 - \frac{hF}{ELby_m}\omega_n, \tag{5}$$

where we introduced the dimensionless extensions $\omega_i = y_i/y_m$. To conclude this procedure, we define the elastic ratio ν and the dimensionless force Q as

$$\nu^2 = \frac{h^2\mu}{L^2E}, \tag{6}$$

$$Q = \frac{Fy_m}{G^f}, \tag{7}$$

finally yielding the mechanical dimensionless energy for the discrete Gibbs ensemble in the form

$$\tilde{\Phi}_G = \frac{1}{n}\sum_{i=1}^{n}\frac{1}{2}(1-\chi_i)\omega_i^2 + \frac{1}{n}\sum_{i=1}^{n}\frac{1}{2}\chi_i + \frac{1}{n}\sum_{i=1}^{n-1}\frac{1}{2}n^2\nu^2(\omega_{i+1}-\omega_i)^2 - Q\omega_n. \tag{8}$$

This is the normalized form of the mechanical energy that will be used in the following developments to introduce the Statistical Mechanics of the system.

Consider then the behavior for $n \to \infty$. In this continuum limit, we introduce the variable $0 \le z \le L$, and we get the limiting value $\tilde{\Phi}_G^\infty$ of the mechanical energy $\tilde{\Phi}_G$, as follows

$$\tilde{\Phi}_G^\infty = \lim_{n\to\infty}\tilde{\Phi}_G = \frac{1}{L}\int_0^L \left\{\frac{1}{2}\left[1-\chi(z)\right]\omega(z)^2 + \frac{1}{2}\chi(z) + \frac{1}{2}L^2\nu^2\left[\omega'(z)\right]^2\right\}dz - Q\omega(L), \tag{9}$$

where $\omega' = d\omega/dz$. Some aspects related to the convergence of the process between discrete and continuous system are discussed below. We can also introduce the dimensionless coordinate $x = z/L$ (with $0 < x < 1$), leading to

$$\tilde{\Phi}_G^\infty = \int_0^1 \left\{\frac{1}{2}\left[1-\chi(x)\right]\omega(x)^2 + \frac{1}{2}\chi(x) + \frac{1}{2}\nu^2\left[\omega'(x)\right]^2\right\}dx - Q\omega(1). \tag{10}$$

So doing, only the elastic ratio ν and the applied dimensionless force Q describe the behavior of the system. Hence, the Gibbs Lagrangian density for the system is

$$\mathcal{L}(x,\omega,\omega') = \frac{1}{2}\left[1-\chi(x)\right]\omega(x)^2 + \frac{1}{2}\chi(x) + \frac{1}{2}\nu^2\left[\omega'(x)\right]^2 - Q\delta(x-1)\omega(x), \tag{11}$$

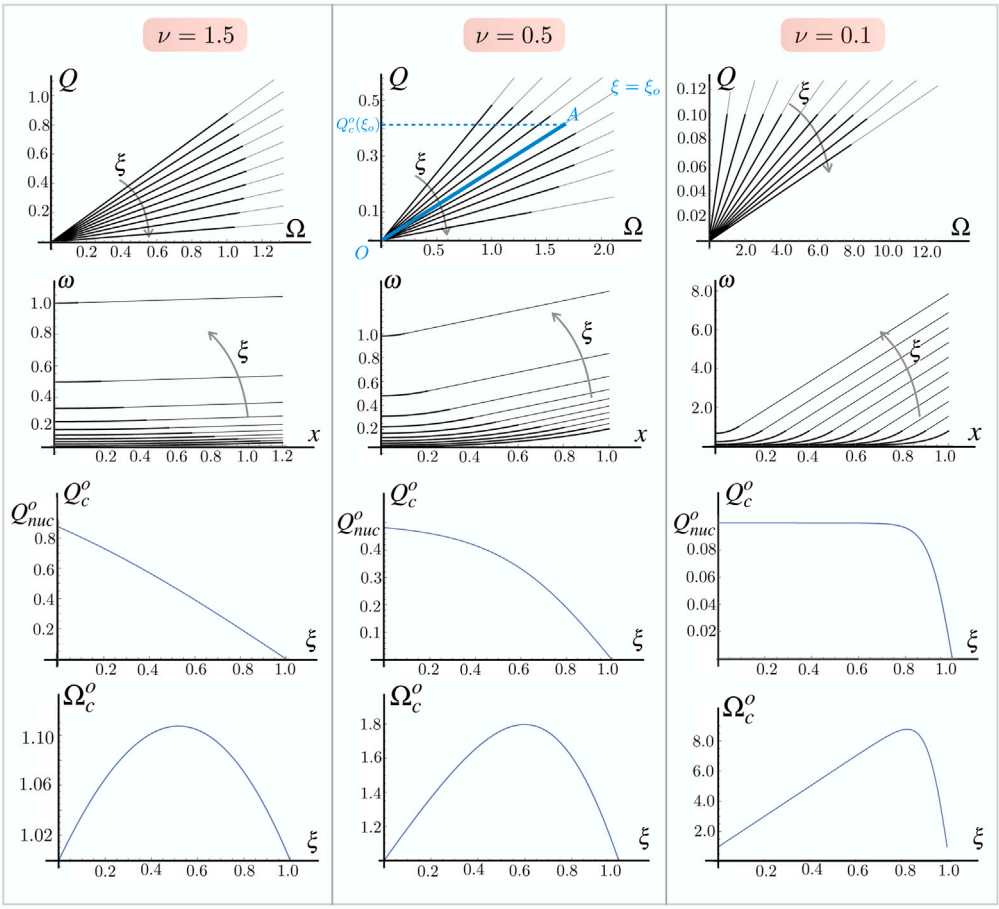

Fig. 2. Decohesion behavior for systems with variable ν, based on the Griffith hypothesis. Upper figures show the overall force–displacement behavior at variable initial detachment $1-\xi$. Bold lines correspond to stable configurations and thin lines to unstable ones, according with the Griffith criterion. The corresponding deformation functions are exhibited in the second row. Third and fourth rows describe the critical force and displacement as a function of the assigned detached fracture ξ.

where δ is the Dirac delta function. It is interesting to observe that the presence of the function χ in the Lagrangian density is reminiscent of the approach used within the phase field models (Miehe et al., 2010; Ren et al., 2019; Zhang et al., 2009). Here, however, we will impose a discontinuous function χ (see below) and we obtain the deformation function ω by minimizing $\tilde{\Phi}_G^\infty$.

Thus, we can calculate the variation $\delta\tilde{\Phi}_G^\infty$ of $\tilde{\Phi}_G^\infty$ in Eq. (10) by considering a perturbed dimensionless extension $\omega(x)+\varepsilon\eta(x)$ and determining $\delta\tilde{\Phi}_G^\infty = \frac{d\tilde{\Phi}_G^\infty(\omega+\varepsilon\eta)}{d\varepsilon}|_{\varepsilon=0}$. Straightforward calculations lead to

$$\delta\tilde{\Phi}_G^\infty = \int_0^1 \left\{\left[1-\chi(x)\right]\omega(x)\eta(x) + \nu^2\omega'(x)\eta'(x)\right\}dx - Q\eta(1). \tag{12}$$

By applying now an integration by parts, we get

$$\delta\tilde{\Phi}_G^\infty = \int_0^1 \left\{\left[1-\chi(x)\right]\omega(x) - \nu^2\omega''(x)\right\}\eta(x)dx - Q\eta(1) + \nu^2\omega'(1)\eta(1) - \nu^2\omega'(0)\eta(0). \tag{13}$$

This variation must be zero for any perturbation $\eta(x)$. Hence, we obtain the (Euler–Lagrange) differential equation

$$\left[1-\chi(x)\right]\omega(x) - \nu^2\omega''(x) = 0, \tag{14}$$

with the boundary conditions

$$\omega'(0) = 0, \tag{15}$$

$$\nu^2\omega'(1) = Q. \tag{16}$$

We remark that from the physical point of view the quantity $\nu^2\omega'(x)$ represents the dimensionless vertical or shear force $t(x)$ at a given point x. By using Eq. (14), we obtain the local equilibrium equation

$$t'(x) = \left[1-\chi(x)\right]\omega(x) > 0, \tag{17}$$

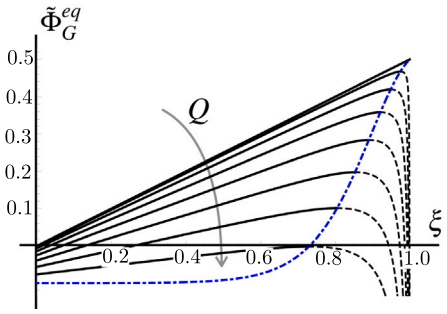

Fig. 3. Total mechanical energy of the Gibbs configuration, minimized with respect to the deformation field ω, versus the detached fraction ξ. Different curves correspond to different applied forces. We adopted $\nu = 0.2$ and $Q \in (0, Q^{nuc})$. The blue dash-dotted curve passes through the energy maximum points, and separates the region where the decohesion front is stopped ($d\tilde{\Phi}_G^{eq}/d\xi > 0$, black solid lines), from the region where the decohesion front propagates ($d\tilde{\Phi}_G^{eq}/d\xi < 0$, black dashed lines).

since $\omega > 0$. As a result, we have that t is a monotonic function increasing from $t(0) = 0$ to $t(1) = Q$, so that $t(x) = \nu^2\omega'(x) > 0$ for $x \in (0, 1)$. Therefore, we obtain that the solutions are always monotonic and, due to our assumption that the breakable links with $\omega < 1$ are intact whereas they are broken when $\omega > 1$, we deduce that the equilibrium solutions are characterized by a single wall geometry. In other words, we can assume that the phase function χ is equal to zero when $0 < x < 1 - \xi$ (attached region) and equal to 1 when $1 - \xi < x < 1$ (detached region). The fraction of the detached region is equal to ξ (with $0 < \xi < 1$). Accordingly, we have to add the continuity of extension and dimensionless force for $x = 1 - \xi$.

The complete definition of the differential problem to be solved is then

$$\omega(x) - \nu^2\omega''(x) = 0 \quad (0 < x < 1 - \xi), \tag{18}$$

$$\omega''(x) = 0 \quad (1 - \xi < x < 1), \tag{19}$$

$$\omega'(0) = 0, \tag{20}$$

$$\omega((1-\xi)^-) = \omega((1-\xi)^+), \tag{21}$$

$$\omega'((1-\xi)^-) = \omega'((1-\xi)^+), \tag{22}$$

$$\nu^2\omega'(1) = Q. \tag{23}$$

The solution can be easily obtained and reads

$$\omega(x) = \frac{Q}{\nu}\frac{\cosh\left(\frac{x}{\nu}\right)}{\sinh\left(\frac{1-\xi}{\nu}\right)}, \tag{24}$$

when $0 < x < 1 - \xi$, and

$$\omega(x) = \frac{Q}{\nu^2}\left[x - 1 + \xi + \nu\coth\left(\frac{1-\xi}{\nu}\right)\right], \tag{25}$$

when $1 - \xi < x < 1$. We underline that this state of deformation corresponds to an assigned percentage ξ of the detached part. Due to the local convexity of the energy all these solutions verify the necessary Legendre stability condition.

In Fig. 2, one can find examples of the equilibrium deformation function $\omega(x)$, corresponding to different size ξ of the detached region. In particular, we obtain, at assigned decohesion fraction ξ, the overall force–displacement relation

$$\Omega(Q, \xi) = \omega(1) = \frac{Q}{\nu^2}\left[\xi + \nu\coth\left(\frac{1-\xi}{\nu}\right)\right]. \tag{26}$$

The total mechanical energy, minimized with respect to the deformation ω, is useful to study the detachment propagation criterion for a given configuration. In particular, we adopt here the criterion based on the classical Griffith hypothesis affirming that the decohesion fronts propagates if the total energy decreases (Griffith, 1921; Pugno, 2021). By substituting Eqs. (24) and (25) in Eq. (10), we get

$$\min_{\omega}\tilde{\Phi}_G^{\infty} =: \tilde{\Phi}_G^{eq}(\xi) = \frac{1}{2}\xi - \frac{1}{2}\frac{1}{\nu^2}\left[\xi + \nu\coth\left(\frac{1-\xi}{\nu}\right)\right]Q^2 = \frac{1}{2}\xi - \frac{1}{2}Q\,\Omega(Q, \xi), \tag{27}$$

which represent the energy of the system with a fixed detached region ξ and a fixed applied dimensionless force Q in the equilibrium state. The behavior of this crucial quantity can be observed in Fig. 3 as a function of ξ for different values of the applied dimensionless force Q. We observe that each curve shows a maximum point. This point, according with the Griffith criterion, separates non propagating and propagating decohesion front regions. Indeed, based on previous results, we can apply the Griffith criterion to

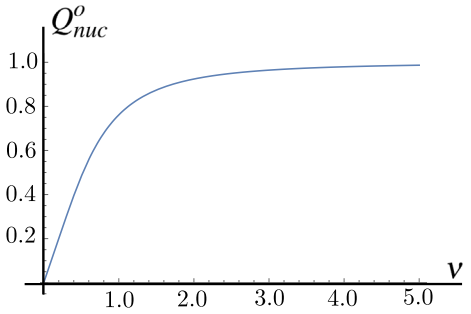

Fig. 4. Dependence of the nucleation threshold from the main parameter ν.

study the evolution of the decohesion front starting from an initial detached percentage ξ. The decohesion front propagates when the total (fracture plus mechanical) energy decreases as the extension of the detached part ξ increases

$$\frac{d}{d\xi}\tilde{\Phi}^{eq}_G < 0 \qquad \Rightarrow \qquad Q\frac{\partial\Omega(Q,\xi)}{\partial\xi} - 1 > 0. \tag{28}$$

The application of this criterion can be seen in Fig. 3. Here the regions where decohesion is advancing and not advancing are identified (separated by the blue dash-dotted line). The calculation of the derivative delivers the decohesion front propagation criterion

$$Q > Q^o_c(\xi) := \nu \tanh\left(\frac{1-\xi}{\nu}\right). \tag{29}$$

This implies that, for a fixed detached region with extension ξ, the deadhesion process proceeds only if the dimensionless force is larger than its threshold value $Q^o_c(\xi)$, prescribed in Eq. (29). This limit force corresponds, by using Eq. (26), to a displacement threshold

$$\Omega > \Omega^o_c(\xi) := 1 + \frac{\xi}{\nu}\tanh\left(\frac{1-\xi}{\nu}\right). \tag{30}$$

Here the superscript "o" recalls that this value represents the limit behavior when thermal effects are neglected, $T \to 0$, and the subscript "c" means that this value is critical in the sense of Griffith. Thus we have the simple relation

$$\Omega^o_c(\xi) = 1 + \frac{\xi}{\nu^2}Q^o_c(\xi). \tag{31}$$

It is worth noticing that in the case of isotensional condition the Griffith propagation criterion always predicts an unstable decohesion front propagation (Zehnder, 2012). Indeed, if we consider an initial detached portion ξ_o and we start increasing the force Q, the decohesion front does not propagates until the critical propagation load $Q^o_c(\xi_o)$ is attained (cyan path O-A in the upper central inset of Fig. 2). On the other hand, since the propagation threshold decreases as the decohesion front propagates ($\frac{dQ^o_c(\xi)}{d\xi} = -\text{sech}^2\left(\frac{1-\xi}{\nu}\right) < 0$, see again Fig. 2), we have $Q > Q^o_c(\xi)$ for the successive configurations $\xi > \xi_o$ with sudden transition to the fully detached state. This behavior is consistent with the condition $d^2\tilde{\Phi}^{eq}_G(\xi)/d\xi^2 < 0$, stating that the second order derivative of the total energy is always negative. This can be further observed in Fig. 3, where we deduce that $\tilde{\Phi}^{eq}_G(\xi)$ is a strictly concave function of ξ (Anderson, 2005).

In Fig. 2 one can find the behavior of $Q^o_c(\xi)$ and $\Omega^o_c(\xi)$. Moreover, the force–extension response given in Eq. (26) is represented together with the Griffith critical load for any value of ξ. We remark that this result is consistent with the so-called de Gennes rupture force, originally developed for DNA molecules (Chauhan et al., 2023; de Gennes, 2001; Mishra et al., 2015; Mosayebi et al., 2015; Singh et al., 2016).

As a particular case, we can also obtain the nucleation criterion for the fully attached configuration

$$Q^o_{nuc} := Q^o_c(0) = \nu \tanh\left(\frac{1}{\nu}\right). \tag{32}$$

The dependence of the nucleation threshold on the relative stiffness parameter ν is exhibited in Fig. 4. As the stiffness of the adhering layer increases the nucleation threshold reaches the asymptotic value $Q = 1$. This results is in agreement with the literature (Puglisi & Truskinovsky, 2013), where the same behavior was obtained on the basis of the local energy minimization in the case of biological adhesion. It is worth noticing that, based on our realistic energetic approach accounting for the real discrete structure at the macro scale, differently from the classical Griffith theory that is not able to predict the nucleation of the fracture, here we are able to determine this fundamental quantity.

It is also interesting to observe that when we are at the critical point $Q = Q^o_c$, we have $\omega(1-\xi) = 1$ ($y = y_m$ when $\omega = 1$). In other words, the Griffith criterion predicts that the decohesion front exactly corresponds to the attainment of the displacement fracture threshold at the decohesion front. While the decohesion criterion here obtained is a purely mechanical result, in the next Section we consider the possible role of thermal fluctuations in such decohesion front propagation conditions.

2.2. Thermal fluctuations effect

To study the effects of thermal fluctuations, we start again from the analysis of the discrete system. For this system we calculate the partition function, representing the statistical sum of the possible states calculated as an integral over all the discrete extensions y_i (see below for details). An alternative approach could have been to operate within the continuum framework using Feynman's path integrals formalism. However, this would have added complexity to the analysis, though it is worth noting that the outcomes should be expected consistent (Kleinert, 1990). For the previous reasons, we rewrite the total mechanical energy in Eq. (8) in matrix form as follows:

$$n\tilde{\Phi}_G = \frac{1}{2}\boldsymbol{\omega}\cdot\boldsymbol{B}_G\boldsymbol{\omega} - Q\boldsymbol{\omega}\cdot\boldsymbol{e}_n + \frac{1}{2}\boldsymbol{\chi}\cdot\mathbf{1}, \tag{33}$$

where $\boldsymbol{\omega} = (\omega_1, \omega_2, \dots, \omega_n) \in \mathbb{R}^n$, $\boldsymbol{\chi} = (\chi_1, \chi_2, \dots, \chi_n) \in \{0,1\}^n$, $\boldsymbol{e}_i$ is the ith element of the canonical basis of $\mathbb{R}^n$, and $\mathbf{1} = \sum_{i=1}^n \boldsymbol{e}_i \in \mathbb{R}^n$. Here, we also introduced the $n\times n$ tridiagonal matrix

$$\boldsymbol{B}_G = n^2\nu^2\boldsymbol{A}_G - n^2\nu^2\left(\boldsymbol{e}_1\otimes\boldsymbol{e}_1 + \boldsymbol{e}_n\otimes\boldsymbol{e}_n\right), \tag{34}$$

where

$$\boldsymbol{A}_G = \begin{bmatrix} a_1 & -1 & 0 & \cdots & 0 \\ -1 & \ddots & \ddots & \ddots & \vdots \\ 0 & \ddots & \ddots & \ddots & 0 \\ \vdots & \ddots & \ddots & \ddots & -1 \\ 0 & \cdots & 0 & -1 & a_n \end{bmatrix}, \tag{35}$$

with $a_i = 2 + (1-\chi_i)/(n^2\nu^2)$, $i = 1, \dots, n$. In Eq. (34), we have separated two terms corresponding to the first and last elements to simplify the form the main (Hessian) matrix $\boldsymbol{A}_G$.[1] It is not difficult to see that Eq. (33) is fully equivalent to Eq. (8). Once we have fixed the vector $\boldsymbol{\chi}$ (the adhesion state) and the applied force Q, we can minimize the energy with respect to the vector $\boldsymbol{\omega}$. Thus, since

$$n\frac{\partial\tilde{\Phi}_G}{\partial\boldsymbol{\omega}} = n^2\nu^2\left(\boldsymbol{A}_G - \boldsymbol{e}_1\otimes\boldsymbol{e}_1 - \boldsymbol{e}_n\otimes\boldsymbol{e}_n\right)\boldsymbol{\omega} - Q\boldsymbol{e}_n, \tag{36}$$

we obtain the equilibrium condition

$$\boldsymbol{\omega} = \frac{Q}{n^2\nu^2}\left(\boldsymbol{A}_G - \boldsymbol{e}_1\otimes\boldsymbol{e}_1 - \boldsymbol{e}_n\otimes\boldsymbol{e}_n\right)^{-1}\boldsymbol{e}_n. \tag{37}$$

This procedure is the discrete counterpart of the variational approach described in the previous section. Then, by Eqs. (33) and (37) we obtain the energy of the equilibrium configurations at assigned decohesion state $\boldsymbol{\chi}$

$$n\min_{\boldsymbol{\omega}}\tilde{\Phi}_G = -\frac{1}{2}\frac{Q^2}{n^2\nu^2}\boldsymbol{e}_n\cdot\left(\boldsymbol{A}_G - \boldsymbol{e}_1\otimes\boldsymbol{e}_1 - \boldsymbol{e}_n\otimes\boldsymbol{e}_n\right)^{-1}\boldsymbol{e}_n + \frac{1}{2}\boldsymbol{\chi}\cdot\mathbf{1}. \tag{38}$$

From now on, we consider the discrete variables χ_i coherently with the adhesion state adopted in the previous section (single domain wall). We remark that in the discrete case at zero temperature these solutions are the only observable ones. However, when thermal effects are considered more decohesion fronts could be observed. Nevertheless, being energetically unfavorable, we may assume that these configurations can be neglected for not too high temperatures (Florio & Puglisi, 2019). Thus, while in the continuous case we suppose that the phase function χ is equal to zero when $0 < x < 1-\xi$ (attached region) and equal to 1 when $1-\xi < x < 1$ (detached region), in the discrete one we impose $\chi_i = 0$ for $1 \le i \le p$ and $\chi_i = 1$ for $p+1 \le i \le n$, where $p = \lfloor(1-\xi)n\rfloor$ (here, $\lfloor z\rfloor$ is the floor function giving the greatest integer less than or equal to z). In these hypotheses, it is important to remark that a very long calculation, not reported here for the sake of brevity, proves that

$$\lim_{n\to\infty}\min_{\boldsymbol{\omega}}\tilde{\Phi}_G = \min_{\omega(x)}\tilde{\Phi}_G^{\infty} = \tilde{\Phi}_G^{eq}, \tag{39}$$

where the right hand side is given in Eq. (27). This indicates that the problem under investigation satisfies the Γ-convergence approach adopted to obtain the correct limit energy functional (Braides, 2002; Maddalena et al., 2009; Maso, 1993). In other words, this implies that the following two procedures are fully equivalent: (i) performing the continuum limit of Eq. (8), and then using the calculus of variation for minimizing Eq. (9) or (10); (ii) minimizing the energy written in a discrete form as in Eq. (33), and then performing the limit for $n\to\infty$ of the obtained minimum value of the mechanical energy. This equivalence will be used in the following steps of our analysis.

We remark that a weaker form of convergence between discrete a continuous model can be easily proved as follows. The discrete solutions for the deformation ω_i converge, for large values of n, to the continuous solutions $\omega = \omega(x)$ previously described. First we consider the equation $\omega_{i+1} - 2\omega_i + \omega_{i-1} = 0$, valid in the region where the film is detached from the substrate, obtained by minimizing Eq. (8) and asking for a constant shear forces between two adiacent elastic springs. Since the difference equation is linear, it has solutions of the type $\omega_i = \lambda^i$. By substituting this form in the equation, we easily get $\lambda^2 - 2\lambda + 1 = 0$, or equivalently $(\lambda-1)^2 = 0$ with the eigenvalue $\lambda = 1$ having multiplicity 2. Thus the difference equation has the general solution $\omega_i = a + bi$, where a and b are

[1] Moreover, we defined the tensor product of two vectors $\boldsymbol{v}$ and $\boldsymbol{w}$ such that $(\boldsymbol{v}\otimes\boldsymbol{w})\boldsymbol{u} = \boldsymbol{w}\cdot\boldsymbol{u}\,\boldsymbol{v}$ for any vector $\boldsymbol{u}$, so that $(\boldsymbol{v}\otimes\boldsymbol{w})_{ij} = v_i w_j$.

arbitrary constants. Obviously, this solution corresponds to the detached part taking a straight shape. Since $x = i/n$ (with $0 < x < 1$), the corresponding continuous solution is $\omega(x) = \tilde{a} + \tilde{b}x$, where $\tilde{a}$ and $\tilde{b}$ are constants, which corresponds to Eq. (25). Similarly, for the attached part, we have to consider the equation $\frac{1}{n^2}\omega_i - v^2\left(\omega_{i+1} - 2\omega_i + \omega_{i-1}\right) = 0$, obtained by minimizing Eq. (8). As before, we can search solution of the form $\omega_i = \lambda^i$. By substitution, we get $\lambda^2 - [2 + 1/(n^2v^2)]\lambda + 1 = 0$. This algebraic equation leads to the solutions

$$\lambda_\pm = 1 + \frac{1}{2n^2v^2} \pm \sqrt{\frac{1}{n^2v^2} + \frac{1}{4n^4v^4}} = 1 + \frac{1}{2n^2v^2} \pm \sqrt{\frac{1}{n^2v^2}\left(1 + \frac{1}{4n^2v^2}\right)}. \tag{40}$$

Here, we can use the approximation $\sqrt{1+x} \sim 1 + x/2$, valid for small values of x. We obtain therefore for large values of n the expression

$$\lambda_\pm \sim 1 + \frac{1}{2n^2v^2} \pm \frac{1}{nv}\left(1 + \frac{1}{8n^2v^2}\right) = 1 \pm \frac{1}{nv} + \frac{1}{2n^2v^2} \pm \frac{1}{8n^3v^3}. \tag{41}$$

The general solution for the discrete case is given by $\omega_i = c\lambda_+^i + d\lambda_-^i$. Again, since $x = i/n$, the particular solution for the continuous case assumes the form

$$\omega(x) = \lambda^i = \lambda^{nx} \sim \left(1 \pm \frac{1}{nv} + \frac{1}{2n^2v^2} \pm \frac{1}{8n^3v^3}\right)^{nx} \sim \left(1 \pm \frac{1}{nv}\right)^{nx} = e^{\pm\frac{x}{v}}. \tag{42}$$

The general solution for the continuous case is then given by $\omega(x) = \tilde{c}e^{+\frac{x}{v}} + \tilde{d}e^{-\frac{x}{v}}$. Thus we see that in the limit of large n we find exactly the same exponential functions as in the continuous case, see Eq. (24). It is not difficult to realize that the specific solution of the discrete case converges to the specific solution of the continuous case, when we fix the boundary conditions at the extremities and the continuity conditions in the internal matching point (for any value of ξ).

We can now start the calculation of the Gibbs partition function. We suppose the system at thermodynamic equilibrium with a thermal bath at temperature T, and then we adopt the canonical distribution of Statistical Mechanics (Gibbs, 1902; Weiner, 1983). We have

$$Z_G(Q, \xi, T) = \int_{\mathbb{R}^n} \exp\left[-\beta\Phi_G(\boldsymbol{y})\right] d\boldsymbol{y} = y_m^n \int_{\mathbb{R}^n} \exp\left[-\tilde{\beta}\tilde{\Phi}_G(\boldsymbol{\omega})\right] d\boldsymbol{\omega}, \tag{43}$$

where $\boldsymbol{y} = (y_1, y_2, \dots, y_n)$, $\boldsymbol{\omega} = (\omega_1, \omega_2, \dots, \omega_n)$, $\beta = 1/(k_B T)$, and k_B is the Boltzmann constant. Moreover, we defined the dimensionless parameter

$$\tilde{\beta} = G^f \beta = \frac{G^f}{k_B T}, \tag{44}$$

measuring the ratio between decohesion and thermal energy, and where G^f is given in Eq. (4). Observe that, coherently with the Griffith approach, we evaluate the partition function at assigned ξ, so that we will obtain the total free energy at assigned ξ, and we can use the condition of decreasing total energy as stability criterion.

From Eqs. (33) and (43), we get

$$Z_G = y_m^n \exp\left[-\frac{\tilde{\beta}}{2n}\boldsymbol{\chi}\cdot\mathbf{1}\right] \int_{\mathbb{R}^n} \exp\left[-\frac{\tilde{\beta}}{n}\left(\frac{1}{2}\boldsymbol{\omega}\cdot\boldsymbol{B}_G\boldsymbol{\omega} - Q\boldsymbol{\omega}\cdot\boldsymbol{e}_n\right)\right] d\boldsymbol{\omega}, \tag{45}$$

where the integration can be performed through the classical Gaussian integral

$$\int_{\mathbb{R}^N} e^{-\boldsymbol{y}\cdot\boldsymbol{M}\boldsymbol{y}} e^{\boldsymbol{w}\cdot\boldsymbol{y}} \mathrm{d}\boldsymbol{y} = \sqrt{\frac{\pi^N}{\det \boldsymbol{M}}} e^{\frac{1}{4}\boldsymbol{w}\cdot\boldsymbol{M}^{-1}\boldsymbol{w}}, \tag{46}$$

which is valid for a positive definite symmetric matrix $\boldsymbol{M}$ and for any vector $\boldsymbol{w}$. We easily get

$$Z_G = y_m^n \sqrt{\frac{(2\pi n)^n}{\tilde{\beta}^n \det \boldsymbol{B}_G}} \exp\left[-\frac{\tilde{\beta}}{2n}\boldsymbol{\chi}\cdot\mathbf{1}\right] \exp\left[\frac{\tilde{\beta}}{2n}\boldsymbol{e}_n\cdot\boldsymbol{B}_G^{-1}\boldsymbol{e}_n Q^2\right]. \tag{47}$$

By using now the definition of the matrix $\boldsymbol{B}_G$ in Eq. (34), we obtain the important result

$$Z_G = y_m^n \sqrt{\frac{(2\pi n)^n}{\tilde{\beta}^n \det \boldsymbol{B}_G}} \exp\left[-\tilde{\beta}\min_{\boldsymbol{\omega}} \tilde{\Phi}_G\right]. \tag{48}$$

Thus, the partition function can be written in terms of the minimized purely mechanical energy of the system. Therefore, in the limit of large values of n, the quantity $\min_{\boldsymbol{\omega}} \tilde{\Phi}_G$ can be substituted with the explicit expression given in Eq. (27), because of the continuum limit stated in Eq. (39). To complete the calculation of Z_G, the asymptotic value of the determinant of the matrix $\boldsymbol{B}_G$ is calculated in Appendix A. The result follows

$$\det \boldsymbol{B}_G \underset{n\to\infty}{\sim} (nv)^{2n-1} \sinh\left(\frac{1-\xi}{v}\right), \tag{49}$$

and allows the explicit calculation of the Gibbs free energy $G = -k_B T \ln Z_G$ (Gibbs, 1902; Manca et al., 2012; Weiner, 1983). Its dimensionless version is

$$\tilde{G} = \frac{G}{G^f} = -\frac{1}{\tilde{\beta}} \ln Z_G \tag{50}$$

and can be written in the explicit form

$$\tilde{G} = \tilde{G}_0 + \frac{1}{2\tilde{\beta}} \ln\left[\sinh\left(\frac{1-\xi}{\nu}\right)\right] + \frac{1}{2}\xi - \frac{1}{2}\frac{1}{\nu^2}\left[\xi + \nu\coth\left(\frac{1-\xi}{\nu}\right)\right] Q^2, \tag{51}$$

where $\tilde{G}_0$ takes into account the non-influential multiplicative constant in front of the partition function Z_G (this term depends on temperature, but not on ξ). It is interesting to observe that the new term in Eq. (51) compared to Eq. (27) comes precisely from the calculation of the determinant of matrix $\boldsymbol{B}_G$, which therefore represents the entropic effects.

Concerning the force–extension behavior, we can write (Manca et al., 2012; Weiner, 1983)

$$\langle\Omega\rangle = -\frac{\partial\tilde{G}}{\partial Q} = \frac{1}{\nu^2}\left[\xi + \nu\coth\left(\frac{1-\xi}{\nu}\right)\right] Q, \tag{52}$$

where $\langle\Omega\rangle = \langle\omega_n\rangle$ is the average vertical extension of the last element of the system, the point at which the force is applied. Thus, the "effective stiffness" of the system $Q/\langle\Omega\rangle$ is still consistent with Eq. (26) as expected, because the energy is convex at assigned values of ξ. As a result, we can rewrite Eq. (51) as

$$\tilde{G} = \tilde{G}_0 + \frac{1}{2\tilde{\beta}} \ln\left[\sinh\left(\frac{1-\xi}{\nu}\right)\right] + \frac{1}{2}\xi - \frac{1}{2} Q\langle\Omega\rangle. \tag{53}$$

The total energy at fixed ξ in Eq. (53) can then be clearly interpreted as the sum, in the order of appearance, of the constant irrelevant term, the entropy term, the fracture energy term, and the mechanical energy.

The obtained closed form expression for the Gibbs free energy is the most important result characterizing the behavior of the isotensional system in contact with a thermal bath at temperature T. In fact, it plays a crucial role in studying the evolution of the decohesion process when thermal effects are relevant. It is well-known from non-equilibrium thermodynamics that the spontaneous physical and/or chemical processes at constant temperature T and constant pressure (in our case we refer to the dimensionless force Q) are characterized by a decreasing Gibbs free energy. Coherently, we here assume that the deadhesion process proceeds (ξ increases) if $\tilde{G}$ decreases. That is, following the Griffith approach, we assume that in a given configuration (with fixed T, Q, and ξ), the detachment process advances if $\partial\tilde{G}/\partial\xi < 0$. In other words, we extend the Griffith's criterion to the adhesion process with thermal effects by replacing the total mechanical energy by the total Gibbs free energy, which takes into account entropic contributions, *i.e.*, thermal fluctuations (Stevens & Guiu, 1991). Observe that, by following the previous procedure, we first minimized out the (convex) variable ω in Eq. (48), and then we considered the criterion for the decohesion front propagation, exactly as in the purely mechanical case when we study the decrease of the equilibrium energy at fixed ξ in Eq. (28).

The derivative of Eq. (51) reads

$$\frac{\partial\tilde{G}}{\partial\xi} = \frac{1}{2} - \frac{1}{2\nu}\coth\left(\frac{1-\xi}{\nu}\right)\left[\frac{1}{\tilde{\beta}} + \frac{Q^2}{\nu}\coth\left(\frac{1-\xi}{\nu}\right)\right], \tag{54}$$

and, therefore, in the configuration with fixed T, Q, and ξ, the deadhesion process advances if

$$Q > Q_c(\xi, T), \tag{55}$$

where

$$Q_c(\xi, T) := Q_c^o(\xi)\sqrt{1 - \frac{1}{\tilde{\beta}Q_c^o(\xi)}}, \tag{56}$$

where we recall that Q_c^o represents the critical load when thermal effects are neglected, see Eq. (29). We can also write the decohesion front propagation condition in the form

$$Q > Q_c(\xi, T) = Q_c^o(\xi)\sqrt{1 - \frac{T}{T_c^G}}, \tag{57}$$

where we identify the critical temperature

$$k_B T_c^G(\xi) = Q_c^o(\xi) G^f. \tag{58}$$

Correspondingly, we can define the critical effective temperature by using Eq. (44)

$$\frac{1}{\tilde{\beta}_c^G(\xi)} := Q_c^o(\xi), \tag{59}$$

in such a way that $\sqrt{1 - \frac{T}{T_c^G(\xi)}} = \sqrt{1 - \frac{\tilde{\beta}_c^G(\xi)}{\tilde{\beta}}}$. Together with the threshold force, we can also introduce the threshold extension $\Omega_c(\xi, T) = \Omega_c^o(\xi)\sqrt{1 - \frac{T}{T_c^G}}$, coming from Eq. (52).

In Fig. 5*a*, we represent the threshold Q_c versus the effective temperature $1/\tilde{\beta}$ for different values of the detached extension ξ, see Eq. (56). We see that the curves describing Q_c always reach zero for a given temperature value. In other words, for any adhesion state there is a value of the temperature able to detach the remaining part of the system without the application of an external force. It is explained by the thermal fluctuations, which favor the exploration of the phase space thus promoting the detachment of the film from the substrate. Finally, the system exhibits a second order phase transition whose critical temperature $T_c^G(\xi)$ has been calculated in closed form. In other terms, we can say that the obtained results generalize the de Gennes maximum pull out force

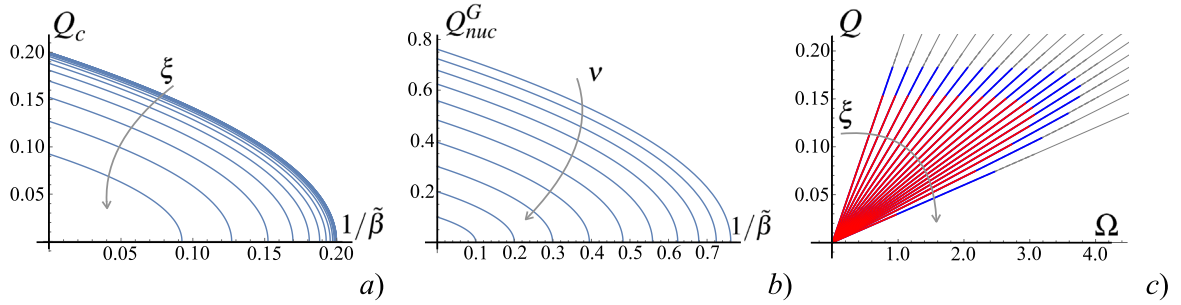

Fig. 5. Decohesion behavior with thermal effect for a system in a soft device. (*a*) Force threshold Q_c for the load-controlled Gibbs deadhesion process, see Eq. (56). The quantity Q_c is plotted versus $1/\tilde{\beta}$ and parametrized by $\xi \in (0, 0.9)$. We adopted the parameter $\nu = 0.2$. (*b*) Nucleation force for different values of the stiffness parameter $\nu = \in (0.1, 1)$ at variable effective temperature $1/\tilde{\beta}$. (*c*) Force–extension relation within the Gibbs ensemble for different values of $\xi = \in (0, 0.9)$ (gray straight lines). For each attachment state characterized by ξ, we represented the breaking threshold corresponding to zero temperature (dashed gray) and two different effective temperatures: $1/\tilde{\beta} = 1/30$ (cold, light blue), and $1/\tilde{\beta} = 1/15$ (warm, dark orange). We adopted the parameter $\nu = 0.2$.

(e.g. for DNA) by introducing thermal effects, which induce a genuine phase transition (Chauhan et al., 2023; de Gennes, 2001; Mishra et al., 2015; Mosayebi et al., 2015; Singh et al., 2016).

In particular, we can study the temperature dependent nucleation force and displacement

$$Q^G_{nuc}(T) = Q^o_{nuc}\sqrt{1 - \frac{T}{T^G_{nuc}}}, \tag{60}$$

$$\Omega^G_{nuc}(T) = \sqrt{1 - \frac{T}{T^G_{nuc}}}, \tag{61}$$

where

$$k_B T^G_{nuc} = G^f Q^o_c(0) \tag{62}$$

represents the critical decohesion temperature for the fully attached system. In Fig. 5*b*, we report the nucleation force as a function of the effective temperature $1/\tilde{\beta}$ for different values of the stiffness parameter ν.

It is also interesting to point out that the critical temperature $T^G_c(\xi)$ of this system depends on the initial detachment state ξ. This is a peculiar property of our solution depending from the fact that we performed an exact continuum limit. Indeed, in other investigations developed by means of the simpler thermodynamic limit, the critical temperature depends only on the intrinsic physical parameters defining the system and not on the initial attachment state (Cannizzo et al., 2021; Cannizzo & Giordano, 2023; De Lorenzo et al., 2015; Florio et al., 2020). In particular, we may observe that the critical temperature is zero for $\xi = 1$ since the system is already fully detached, and T^G_c increases when ξ decreases, achieving the maximum value for $\xi = 0$, see Eq. (58). In other words, the critical temperature is a decreasing function of ξ, see again Eq. (58). Moreover, it is easy to verify that at fixed temperature Q_c, in Eq. (56), decreases as ξ increases (in the same way as Q^o_c that decreases as ξ increases) so that again at any given T the Griffith detachment propagation is unstable in the Gibbs ensemble (Zehnder, 2012). In other terms, the Gibbs free energy is always strictly concave for any value of the temperature.

In Fig. 5*c*, the straight lines correspond to the force extension relation in Eq. (52), for different values of the attachment variable ξ. In the same plot, we represented the breaking thresholds for any value of ξ and for two different effective temperatures $1/\tilde{\beta}$. We remark the important effect of the temperature in decreasing the threshold force at given adhesion state ξ.

3. Displacement-controlled Helmholtz ensemble: hard device

In this Section, we delve into the study of adhesion and deadhesion processes controlled by specifying the extension Ω of the right-end terminal of the film. Drawing an analogy with a constant-volume system in Statistical Mechanics, we refer to this configuration as the Helmholtz ensemble. From an experimental perspective, this setup is achieved using an hard device, indicating that its intrinsic elastic stiffness greatly exceeds that of the film. Similar to our approach with the Gibbs ensemble, we initially examine the purely mechanical model and subsequently incorporate the influence of thermal fluctuations.

3.1. Purely mechanical deadhesion

We adopt the same notations introduced for the Gibbs ensemble and we substitute the applied force F with the prescribed extension y_n. The energy of the system is

$$\Phi_H = \frac{1}{2}\sum_{i=1}^{n}(1 - \chi_i)k_t y_i^2 + \frac{1}{2}\sum_{i=1}^{n}\chi_i k_t y_m^2 + \frac{1}{2}\sum_{i=1}^{n-1}k_\ell (y_{i+1} - y_i)^2, \tag{63}$$

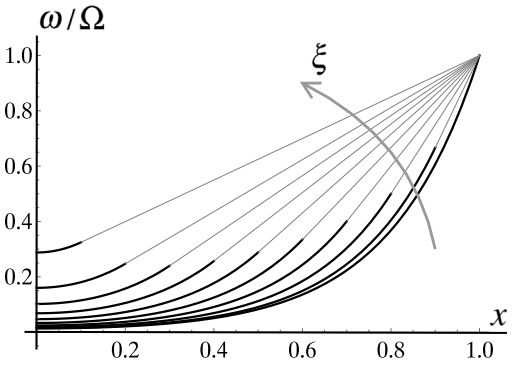

Fig. 6. Example of state of deformation $\omega(x)/\Omega$ for the displacement-controlled Helmholtz ensemble. We implemented Eqs. (73) and (74) with the parameters $\nu = 0.2$ and $\xi \in (0, 0.9)$. Thick lines correspond to the attached region while thin ones correspond to the detached region.

where $y_n = \Omega y_m$ is fixed. Here, Ω is the dimensionless applied extension, see Fig. 1a. As before, we impose the parameters k_t and k_ℓ as in Eq. (2) and (3) to have the correct continuum rescaling. Hence, we introduce the dimensionless version $\tilde{\boldsymbol{\Phi}}_H$ of the energy $\boldsymbol{\Phi}_H$

$$\tilde{\boldsymbol{\Phi}}_H = \frac{\boldsymbol{\Phi}_H}{G^f} = \frac{1}{n}\sum_{i=1}^{n}\frac{1}{2}(1-\chi_i)\omega_i^2 + \frac{1}{n}\sum_{i=1}^{n}\frac{1}{2}\chi_i + \frac{1}{n}\sum_{i=1}^{n-1}\frac{1}{2}n^2\nu^2(\omega_{i+1}-\omega_i)^2, \tag{64}$$

where, now, we impose $\omega_n = \Omega$. In the continuum limit, for $n \to \infty$, we introduce the variable $0 \le x \le 1$ and we get the limiting value $\tilde{\boldsymbol{\Phi}}_H^{\infty}$ of the energy $\tilde{\boldsymbol{\Phi}}_H$

$$\tilde{\boldsymbol{\Phi}}_H^{\infty} = \int_0^1 \left\{ \frac{1}{2}\left[1-\chi(x)\right]\omega(x)^2 + \frac{1}{2}\chi(x) + \frac{1}{2}\nu^2\left[\omega'(x)\right]^2 \right\} dx. \tag{65}$$

Therefore, the Helmholtz Lagrangian density for the system is

$$\mathcal{L}(x,\omega,\omega') = \frac{1}{2}\left[1-\chi(x)\right]\omega(x)^2 + \frac{1}{2}\chi(x) + \frac{1}{2}\nu^2\left[\omega'(x)\right]^2, \tag{66}$$

where $\omega' = d\omega/dx$. As before, we obtain that the equilibrium solutions are monotonic ($\omega' > 0$) so that we may restrict the analysis to the case of a single domain wall configuration with $\chi(x) = 0$ when $0 < x < 1-\xi$ (attached region) and $\chi(x) = 1$ when $1-\xi \le x \le 1$ (detached region). Hence, we obtain the Euler–Lagrange equilibrium condition

$$\omega(x) - \nu^2\omega''(x) = 0 \quad (0 < x < 1-\xi), \tag{67}$$

$$\omega''(x) = 0 \quad (1-\xi < x < 1), \tag{68}$$

$$\omega'(0) = 0, \tag{69}$$

$$\omega((1-\xi)^-) = \omega((1-\xi)^+), \tag{70}$$

$$\omega'((1-\xi)^-) = \omega'((1-\xi)^+), \tag{71}$$

$$\omega(1) = \Omega. \tag{72}$$

The solution can be easily obtained and reads

$$\omega(x) = \frac{\nu\cosh\left(\frac{x}{\nu}\right)}{\nu\cosh\left(\frac{1-\xi}{\nu}\right) + \xi\sinh\left(\frac{1-\xi}{\nu}\right)}\Omega, \tag{73}$$

for $0 < x < 1-\xi$, and

$$\omega(x) = \frac{\nu\cosh\left(\frac{1-\xi}{\nu}\right) + (x-1+\xi)\sinh\left(\frac{1-\xi}{\nu}\right)}{\nu\cosh\left(\frac{1-\xi}{\nu}\right) + \xi\sinh\left(\frac{1-\xi}{\nu}\right)}\Omega, \tag{74}$$

for $1-\xi < x < 1$. In Fig. 6, one can find examples of shapes of the deformation functions in the Helmholtz case, induced by different extensions ξ of the detached region. We can obtain the equilibrium force–elongation relation

$$Q(\Omega,\xi) = \nu^2\omega'(1) = \frac{Q_c^o(\xi)}{\Omega_c^o(\xi)}\Omega, \tag{75}$$

where $Q_c^o(\xi)$ and $\Omega_c^o(\xi)$ are defined as in the Gibbs's case, see Eqs. (29) and (30). Of course, Eq. (75) is in perfect agreement with Eq. (26).

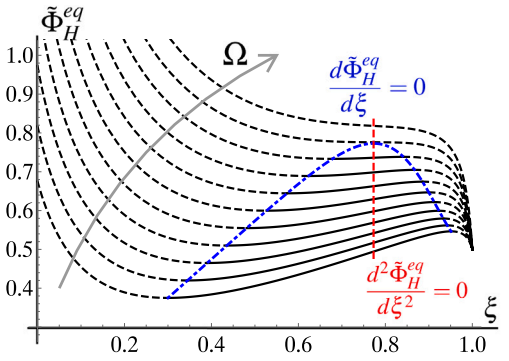

Fig. 7. Total mechanical energy of the Helmholtz configuration, minimized with respect to the deformation field ω, versus the detached fraction ξ. Different curves correspond to different prescribed displacements Ω. We adopted $\nu = 0.15$ and $\Omega \in (3, 5.4)$. The blue dash-dotted curves pass through the energy minimum points and energy maximum points, and separates the regions where the decohesion front is stopped ($d\tilde{\Phi}_G^{eq}/d\xi > 0$, black solid lines), from the regions where the decohesion front propagates ($d\tilde{\Phi}_G^{eq}/d\xi < 0$, black dashed lines). Moreover, the red line passes through the inflection points ($d^2\tilde{\Phi}_G^{eq}/d\xi^2 = 0$, corresponding to ξ_{max}, see the main text) of the energy curves and separates the stable zone (convex energy) from the unstable zone (concave energy).

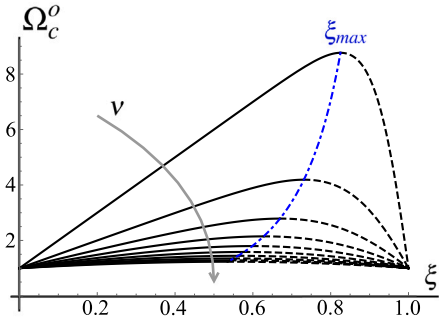

Fig. 8. Dependence of the decohesion threshold Ω_c^o on the decohesion fraction ξ for variable values of the non dimensional stiffness parameter ν, within the displacement-controlled Helmholtz ensemble. We have indicated the location of the maxima, which separates the stable region from the unstable region.

As we have already done in the isotensional case, also for the isometric configuration we can substitute Eqs. (73) and (74) in Eq. (65) to get the minimized energy of the system with fixed detached extension ξ. After straightforward calculations, we obtain

$$\min_{\omega(x)} \tilde{\Phi}_H^{\infty} =: \tilde{\Phi}_H^{eq}(\xi) = \frac{1}{2}\xi + \frac{1}{2}\nu^2 \frac{1}{\xi + \nu \coth\left(\frac{1-\xi}{\nu}\right)} \Omega^2 = \frac{1}{2}\xi + \frac{1}{2} Q(\Omega, \xi)\, \Omega. \tag{76}$$

Interestingly enough, we can underline a mathematical relationship between the load-controlled Gibbs minimized mechanical energy $\tilde{\Phi}_G^{eq} = \min_\omega \tilde{\Phi}_G^{\infty}$ and the displacement-controlled Helmholtz minimized energy $\tilde{\Phi}_H^{eq} = \min_\omega \tilde{\Phi}_H^{\infty}$. From the Gibbs deformation given in Eq. (25), we deduce that $\omega(1) = \left[\xi + \nu \coth\left(\frac{1-\xi}{\nu}\right)\right] Q/\nu^2$, and we can assign this value to the variable Ω of the Helmholtz configuration. So doing, we easily prove that

$$\tilde{\Phi}_G^{eq} = \min_{\omega(x)} \tilde{\Phi}_G^{\infty} = \min_{\omega(x)} \tilde{\Phi}_H^{\infty} - Q\Omega = \tilde{\Phi}_H^{eq} - Q\Omega, \tag{77}$$

which represents a Legendre transformation between Helmholtz and Gibbs configurations, as in classical continuum thermodynamics approaches (Manca et al., 2012; Weiner, 1983).

The minimized energy in Eq. (76), as before, can be used to apply the Griffith criterion and determine the decohesion front propagation condition. In the hard device case the Griffith criterion reads

$$\frac{d}{d\xi}\tilde{\Phi}_H^{eq} < 0 \rightarrow \Omega \frac{\partial Q(\Omega, \xi)}{\partial \xi} + 1 < 0 \tag{78}$$

which can be rewritten as

$$\Omega > \Omega_c^o(\xi) := \Omega_c^o(\xi) = 1 + \frac{\xi}{\nu^2} Q_c^o(\xi), \tag{79}$$

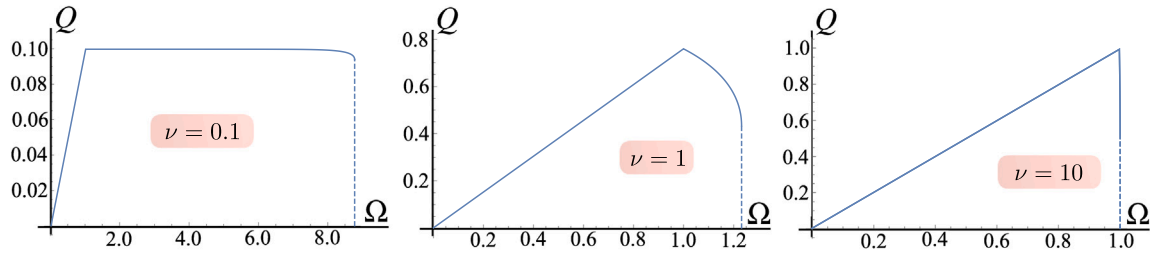

Fig. 9. Decohesion behavior in the displacement-controlled Helmholtz ensemble for different values of the stiffness parameter ν, regulating the ductility of the process. Here we studied the nucleation behavior when the system is loaded starting from the fully attached configuration $\xi = 0$.

with the same threshold as in Eq. (30). Thus, for a fixed detached region with extension ξ, the detachment proceeds only if the prescribed extension Ω is larger than its threshold value Ω_c^o. Once again, this corresponds to the same value of the critical force obtained in Eq. (29)

$$Q(\Omega_c^o(\xi), \xi) = \nu^2 \omega'(1) = Q_c^o(\xi), \tag{80}$$

for the Gibbs case. The obtained Griffith result can be observed in Fig. 7, where the mechanical energy is plotted as function of the detached fraction ξ. It can be seen as the displacement-controlled counterpart of Fig. 3, corresponding to the load-controlled case. Three regions can be identified (when Ω is below a certain threshold): in the first and third regions the energy decreases with ξ, and in the second, the middle region, the energy increases with ξ. The frontiers between these regions correspond to the Griffith's decohesion advance criterion. In addition, two zones are identified where the energy is concave and convex, separated by an inflection point. They correspond to unstable and stable regimes, respectively, as discussed below. Observe that for a certain value of the prescribed displacement Ω, the two frontiers representing Griffith's criterion converge at a single point corresponding to $\xi = \xi_{max}$. This indicates that for any prescribed displacement Ω exceeding this threshold (see, for instance, the upper curve), the energy function is always decreasing and therefore the decohesion front always propagates, because the Griffith's propagation criterion is always fulfilled.

Moreover, it is important to point out that the decohesion behavior is strongly different for the Gibbs and Helmholtz ensembles in terms of the possibility of a coherent quasi-static propagation of the decohesion front as the external load Ω is increased. Indeed, in the case of assigned force Q, when the system attains the threshold $Q_c^o(\xi)$ (and in particular Q_{nuc}^o in the case of zero initial detachment), it always suddenly 'jumps' to the fully detached state. This instability corresponds to the strictly concave character of the Gibbs energy function, see Fig. 3. On the other hand, for the system detached with an hard device (Helmholtz ensemble), the quantity Ω_c^o is a non-monotonic function of ξ (see Fig. 8), exhibiting a maximum point for a specific value of ξ that can be obtained by solving the transcendental equation

$$\xi_{max} = \frac{1}{2}\nu \sinh\left[\frac{2(1-\xi_{max})}{\nu}\right]. \tag{81}$$

Thus, if the initial detachment fraction is $\xi < \xi_{max}$, the decohesion process starts at $\Omega_c^o(\xi)$ and the front coherently propagates until the value $\Omega_c^o(\xi_{max})$ is attained, and the remaining attached region suddenly detach. The decohesion is instead fragile for $\xi > \xi_{max}$. This is consistent with the plot of the Helmholtz energy function shown in Fig. 7. Indeed the energy curve is convex, $d^2\tilde{\Phi}_H^{eq}(\xi)/d\xi^2 > 0$, for $\xi < \xi_{max}$, leading to decohesion stability, and the curve is concave, $d^2\tilde{\Phi}_H^{eq}(\xi)/d\xi^2 < 0$, for $\xi > \xi_{max}$, leading to decohesion instability. Note that the red dashed line joining the inflection points is a vertical line since ξ_{max} depends only on ν, which is held constant in Fig. 7.

The decohesion behavior, starting from a configuration with $\xi = 0$ and variable values of the stiffness parameter ν are exhibited in Fig. 9. We observe that the system undergoes a ductile to fragile transition as ν increases. The influence of the initial detached fraction, which induces a decreasing of the system ductility, is instead described in Fig. 10.

To conclude, as a check of our calculations, we can underline that when we are at the stability limit $\Omega = \Omega_c^o$, we have $\omega(1-\xi) = 1$. This means that for $x = 1-\xi$, at the point of contact between the intact and broken regions, the extension exactly equals the fracture threshold as expected (indeed, $y = y_m$ when $\omega = 1$). In the next Section, we generalize these purely mechanical results with the introduction of thermal fluctuations.

3.2. Thermal fluctuations effect

In order to introduce the effect of thermal fluctuations on the isometric adhesion process, we start again our analysis with the discrete version of the energy in Eq. (64). In this equation, we have to impose the extension of the right end of the chain, namely we fix $\omega_n = \Omega$. For this reason, the phase space in this case is composed by vectors with $n-1$ components: $\boldsymbol{\omega} = (\omega_1, \omega_2, \dots, \omega_{n-1}) \in \mathbb{R}^{n-1}$. The dimensionless energy can be rewritten in matrix form as follows

$$n\tilde{\Phi}_H = \frac{1}{2}\boldsymbol{\omega} \cdot \boldsymbol{B}_H \boldsymbol{\omega} + \frac{1}{2}(1 - \chi_n + n^2\nu^2)\Omega^2 + \frac{1}{2}\chi \cdot \mathbf{1} - n^2\nu^2\Omega\boldsymbol{\omega} \cdot \boldsymbol{e}_{n-1}, \tag{82}$$

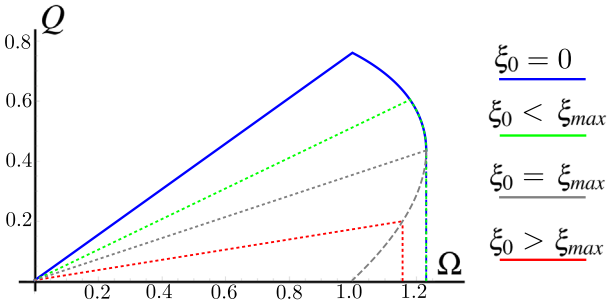

Fig. 10. Decohesion behavior for a system with variable initial detached extension ξ_0 within the displacement-controlled Helmholtz ensemble. Here, we assumed $\nu = 1$.

where $\chi = (\chi_1, \chi_2, \dots, \chi_n) \in \mathbb{R}^n$, $\boldsymbol{e}_i$ is the ith element of the canonical basis of $\mathbb{R}^{n-1}$, and $\mathbf{1} = (1, 1, \dots, 1) \in \mathbb{R}^n$. Here, we also introduced the $(n-1)\times(n-1)$ tridiagonal matrix

$$\boldsymbol{B}_H = n^2\nu^2\boldsymbol{A}_H - n^2\nu^2\boldsymbol{e}_1 \otimes \boldsymbol{e}_1, \tag{83}$$

where

$$\boldsymbol{A}_H = \begin{bmatrix} a_1 & -1 & 0 & \cdots & 0 \\ -1 & \ddots & \ddots & \ddots & \vdots \\ 0 & \ddots & \ddots & \ddots & 0 \\ \vdots & \ddots & \ddots & \ddots & -1 \\ 0 & \cdots & 0 & -1 & a_{n-1} \end{bmatrix}, \tag{84}$$

with $a_i = 2 + (1-\chi_i)/(n^2\nu^2)$, $i = 1, \dots, n-1$. With these assumptions, Eq. (82) is completely equivalent to Eq. (64). We can therefore proceed with the energy minimization at fixed detached fraction as described in the Gibbs ensemble, by considering, for the moment, an arbitrary vector χ. To begin, we calculate the derivative

$$n\frac{\partial\tilde{\Phi}_H}{\partial\boldsymbol{\omega}} = n^2\nu^2\left(\boldsymbol{A}_H - \boldsymbol{e}_1 \otimes \boldsymbol{e}_1\right)\boldsymbol{\omega} - n^2\nu^2\Omega\boldsymbol{e}_{n-1} \tag{85}$$

and we obtain the equilibrium deformation

$$\boldsymbol{\omega} = \Omega\left(\boldsymbol{A}_H - \boldsymbol{e}_1 \otimes \boldsymbol{e}_1\right)^{-1}\boldsymbol{e}_{n-1} \tag{86}$$

that we can substitute Eq. (86) in Eq. (82) to obtain the equilibrium energy

$$n\min_{\boldsymbol{\omega}}\tilde{\Phi}_H = -\frac{1}{2}\Omega^2n^2\nu^2\boldsymbol{e}_{n-1}\cdot\left(\boldsymbol{A}_H - \boldsymbol{e}_1 \otimes \boldsymbol{e}_1\right)^{-1}\boldsymbol{e}_{n-1} + \frac{1}{2}(1 - \chi_n + n^2\nu^2)\Omega^2 + \frac{1}{2}\chi\cdot\mathbf{1}. \tag{87}$$

As before, we consider the discrete variables χ_i coherently with the adhesion state adopted in the continuous analysis. It means that we impose $\chi_i = 0$ for $1 \le i \le p$ and $\chi_i = 1$ for $p+1 \le i \le n$, where $p = \lfloor(1-\xi)n\rfloor$. Under these hypotheses, as discussed for the Gibbs configuration, we can prove that

$$\lim_{n\to\infty}\min_{\boldsymbol{\omega}}\tilde{\Phi}_H = \min_{\omega}\tilde{\Phi}_H^{\infty} = \tilde{\Phi}_H^{eq}. \tag{88}$$

Again, this condition indicates the respect of the Γ-convergence condition for our energy functional (Braides, 2002; Maso, 1993).

These premises allow for the calculation of the Helmholtz partition function. As before, we suppose the system at equilibrium (temperature T and ξ fixed) and we adopt the canonical distribution of the Statistical Mechanics (Gibbs, 1902; Weiner, 1983). We get

$$Z_H(\Omega, \xi, T) = \int_{\mathbb{R}^{n-1}}\exp\left[-\beta\Phi_H(\boldsymbol{y})\right]d\boldsymbol{y} = y_m^{n-1}\int_{\mathbb{R}^{n-1}}\exp\left[-\tilde{\beta}\tilde{\Phi}_H(\boldsymbol{\omega})\right]d\boldsymbol{\omega}. \tag{89}$$

From Eqs. (82) and (89), we get

$$Z_H = y_m^{n-1}\exp\left(-\tilde{\beta}\Theta\right)\int_{\mathbb{R}^{n-1}}\exp\left[-\frac{\tilde{\beta}}{n}\left(\frac{1}{2}\boldsymbol{\omega}\cdot\boldsymbol{B}_H\boldsymbol{\omega} - n^2\nu^2\Omega\boldsymbol{\omega}\cdot\boldsymbol{e}_{n-1}\right)\right]d\boldsymbol{\omega}, \tag{90}$$

where

$$\Theta = \frac{1}{2}(1 - \chi_n + n^2\nu^2)\Omega^2 + \frac{1}{2}\chi\cdot\mathbf{1} \tag{91}$$

has been introduced to deal with more compact expressions. As already done within the Gibbs ensemble, the integration can be performed through the classical Gaussian property stated in Eq. (46). We eventually obtain

$$Z_H = y_m^{n-1}\sqrt{\frac{(2\pi n)^{n-1}}{\tilde{\beta}^{n-1}\det\boldsymbol{B}_H}}\exp\left(-\tilde{\beta}\Theta\right)\exp\left[\frac{\tilde{\beta}}{2n}n^4\nu^4\boldsymbol{e}_{n-1}\cdot\boldsymbol{B}_H^{-1}\boldsymbol{e}_{n-1}\Omega^2\right]$$

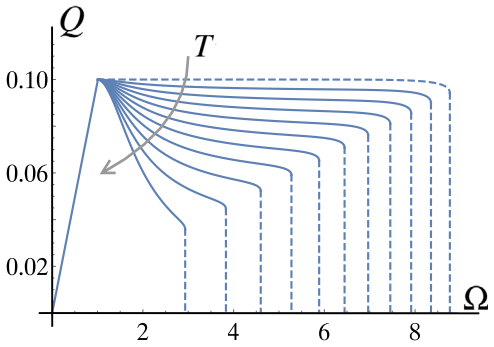

Fig. 11. Decohesion behavior at variable temperature within the displacement-controlled Helmholtz ensemble. The upper dashed line corresponds to the mechanical limit ($T = 0$). We adopted the parameter $\nu = 0.1$. We consider here the nucleation behavior, *i.e.* we assume that loading starts from the fully attached state $\xi = 0$.

$$= y_m^{n-1} \sqrt{\frac{(2\pi n)^{n-1}}{\tilde{\beta}^{n-1} \det \boldsymbol{B}_H}} \exp\left[-\tilde{\beta} \min_{\boldsymbol{\omega}} \tilde{\boldsymbol{\Phi}}_H\right], \tag{92}$$

where we used the definition of the matrix $\boldsymbol{B}_H$ in Eq. (83), and the minimized energy given in Eq. (87). Importantly, in the limit of large values of n, the quantity $\min_{\boldsymbol{\omega}} \tilde{\boldsymbol{\Phi}}_H$ can be substituted with the explicit expression given in Eq. (76), thanks to the Γ-convergence property stated in Eq. (88). The asymptotic behavior of the determinant of the matrix $\boldsymbol{B}_H$ is studied in Appendix B. The result is

$$\det \boldsymbol{B}_H \underset{n\to\infty}{\sim} (n\nu)^{2n-2} \left[\frac{\xi}{\nu} \sinh\left(\frac{1-\xi}{\nu}\right) + \cosh\left(\frac{1-\xi}{\nu}\right)\right] \tag{93}$$

and is useful to calculate the Helmholtz free energy $F = -k_B T \ln Z_H$ (Gibbs, 1902; Manca et al., 2012; Weiner, 1983). As in previous cases, we adopt the dimensionless version given by

$$\tilde{F} = \frac{F}{G^f} = -\frac{1}{\tilde{\beta}} \ln Z_H, \tag{94}$$

and we obtain

$$\tilde{F} = \tilde{F}_0 + \frac{1}{2\tilde{\beta}} \ln\left\{\sinh\left(\frac{1-\xi}{\nu}\right)\left[\xi + \nu \coth\left(\frac{1-\xi}{\nu}\right)\right]\right\} + \frac{1}{2}\xi + \frac{1}{2}\nu^2 \frac{1}{\xi + \nu \coth\left(\frac{1-\xi}{\nu}\right)} \Omega^2, \tag{95}$$

where $\tilde{F}_0$ takes into account the non-influential multiplicative constant in front of the partition function Z_H (this term depends on temperature but cannot depend on ξ). The explicit form of the Helmholtz free energy represents an important result because it allows us to develop the new version of the stability/instability criterion for the Helmholtz adhesion phenomenon.

First, we observe that by partial minimization of the energy at fixed ξ with respect to Ω, one obtains

$$\langle Q \rangle = \frac{\partial \tilde{F}}{\partial \Omega} = \frac{Q_c^o(\xi)}{\Omega_c^o(\xi)} \Omega, \tag{96}$$

which corresponds to the force–extension relation stated in Eqs. (26) and (75).

In analogy with the previous Gibbs analysis, to extend the Griffith criterion, we recall from non-equilibrium thermodynamics that the spontaneous physical and/or chemical processes at constant temperature T and fixed extension (in our case we refer to the dimensionless variable Ω) are characterized by a decreasing Helmholtz free energy. Therefore, again by extending the Griffith approach to the case when thermal fluctuations are considered, in our system the deadhesion process advances (ξ increases) if $\tilde{F}$ decreases. That is, the Griffith propagation condition is fulfilled (with fixed T, Ω, and ξ) if $\partial \tilde{F}/\partial \xi < 0$. As before, Griffith's criterion applied to the adhesion process remains valid but the total energy must be replaced by the Helmholtz free energy, which considers entropic contributions, or equivalently, thermal fluctuations (Stevens & Guiu, 1991). The derivative of Eq. (95) reads

$$\frac{\partial \tilde{F}}{\partial \xi} = -\frac{1}{2\tilde{\beta}} \frac{\xi}{\nu} \frac{\coth\left(\frac{1-\xi}{\nu}\right)}{\xi + \nu \coth\left(\frac{1-\xi}{\nu}\right)} + \frac{1}{2} - \frac{1}{2}\nu^2 \Omega^2 \frac{\coth^2\left(\frac{1-\xi}{\nu}\right)}{\left[\xi + \nu \coth\left(\frac{1-\xi}{\nu}\right)\right]^2}. \tag{97}$$

The Griffith propagation threshold of a given configuration is therefore assigned by

$$\Omega > \Omega_c(\xi, T), \tag{98}$$

where

$$\Omega_c(\xi, T) = \left[1 + \frac{\xi}{\nu} \tanh\left(\frac{1-\xi}{\nu}\right)\right] \sqrt{1 - \frac{\xi}{\tilde{\beta}\nu^2} \frac{1}{1 + \frac{\xi}{\nu} \tanh\left(\frac{1-\xi}{\nu}\right)}} = \Omega_c^o \sqrt{1 - \frac{\xi}{\tilde{\beta}\nu^2 \Omega_c^o}}. \tag{99}$$

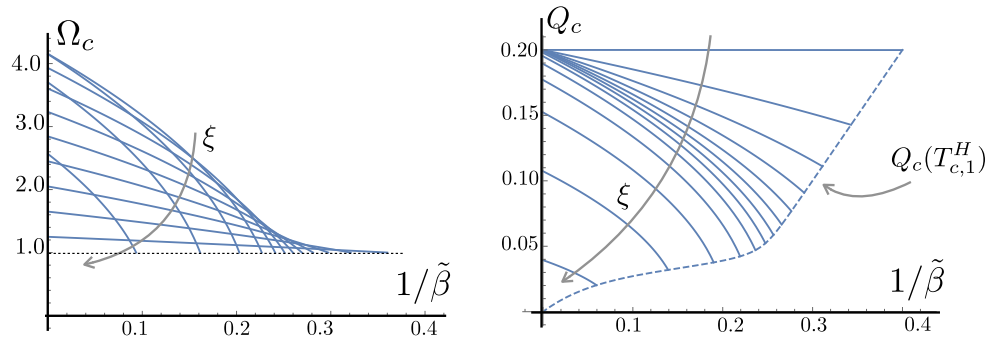

Fig. 12. Behavior of the displacement and force thresholds Ω_c and Q_c for the displacement-controlled Helmholtz deadhesion process. The quantities Ω_c and Q_c are plotted versus $1/\tilde{\beta}$ and parametrized by $\xi \in (0,1)$. We adopted the parameter $\nu = 0.2$.

Thus, the square root modifies the purely mechanical threshold in order to introduce entropic effects. A typical decohesion behavior is shown in Fig. 11 where, starting from $\xi = 0$, we considered the threshold stated in Eq. (99). It follows that the curves represent the real decohesion trajectories followed by the system with an increasing extension Ω at temperature T. Of course, we can associate the critical displacement with the critical force defined as follows

$$Q_c(\xi, T) = \frac{Q_c^o(\xi)}{\Omega_c^o(\xi)} \Omega_c(\xi, T), \tag{100}$$

where we used Eq. (96). In such a way we determine a temperature dependent decohesion behavior in analytical form.

We want to interpret these results again in terms of phase transitions. Typically, a phase transition is seen when, at a certain temperature, known as the critical temperature, the free system (without mechanical actions) detaches in response to thermal fluctuations. In the Helmholtz ensemble, the system is not really free because there is the fixed end and therefore different interpretations of phase transition can be given. Indeed, for any value of a real parameter δ, Eq. (99) can be rewritten as

$$\Omega_c = \sqrt{\delta^2 + \left[(\Omega_c^o)^2 - \delta^2 - \frac{\xi \Omega_c^o}{\tilde{\beta}\nu^2}\right]}, \tag{101}$$

from which we get

$$\Omega_c(\xi, T) = \sqrt{\delta^2 + \left[(\Omega_c^o)^2 - \delta^2\right]\left(1 - \frac{\xi \Omega_c^o}{\tilde{\beta}\nu^2\left[(\Omega_c^o)^2 - \delta^2\right]}\right)}, \tag{102}$$

or

$$\sqrt{\Omega_c^2 - \delta^2} = \sqrt{(\Omega_c^o)^2 - \delta^2}\sqrt{1 - \frac{\xi \Omega_c^o}{\tilde{\beta}\nu^2\left[(\Omega_c^o)^2 - \delta^2\right]}}. \tag{103}$$

This new form reveals critical behavior, specifically a phase transition.[2] We can therefore define the critical temperature $T^H_{c,\delta}$, and the effective critical temperature $1/\tilde{\beta}^H_{c,\delta}$ as

$$\frac{G^f}{\tilde{\beta}^H_{c,\delta}} = k_B T^H_{c,\delta} := \frac{\nu^2[(\Omega_c^o)^2 - \delta^2]G^f}{\xi \Omega_c^o}, \tag{104}$$

so that Eq. (103) delivers

$$\sqrt{\Omega_c^2 - \delta^2} = \sqrt{(\Omega_c^o)^2 - \delta^2}\sqrt{1 - \frac{T}{T^H_{c,\delta}}}. \tag{105}$$

The critical value $T^H_{c,\delta}(\xi)$ has the interesting meaning of a temperature such that at a given ξ and assigned δ the system undergoes spontaneous detachment. In particular, if we assume for example that $\delta = 0$, we obtain

$$\Omega_c(\xi, T) = \Omega_c^o\sqrt{1 - \frac{\xi}{\tilde{\beta}\nu^2\Omega_c^o}} = \Omega_c^o\sqrt{1 - \frac{T}{T^H_{c,0}}}, \tag{106}$$

[2] We remark that while it allows a clear interpretation in terms of phase transition, the new form in Eq. (103) has a smaller domain of definition than Eq. (102).

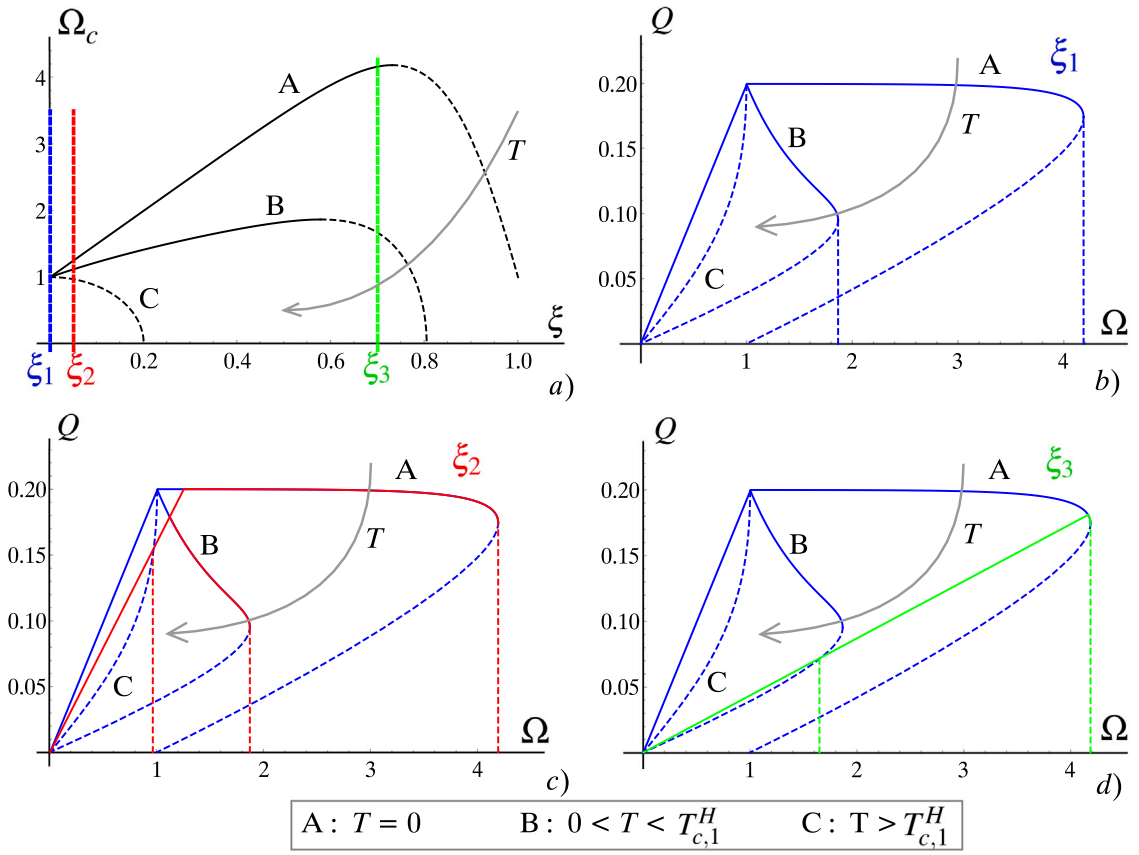

Fig. 13. Decohesion behavior with variable temperature and variable initial detached fraction. (*a*) critical displacement threshold Ω_c as function of the initial detached portion ξ. The curves A, B and C are obtained for three different temperatures, namely $T = 0$ (mechanical system), $0 < T < T^H_{c,1}$, and $T > T^H_{c,1}$, respectively. Three different initial detached portion are considered: $\xi_1 = 0$ (nucleation behavior), $\xi_2 > \xi_1$, and $\xi_3 > \xi_2$. For each initial detached fraction we plot the force–displacement decohesion behavior in (*b*), (*c*) and (*d*).

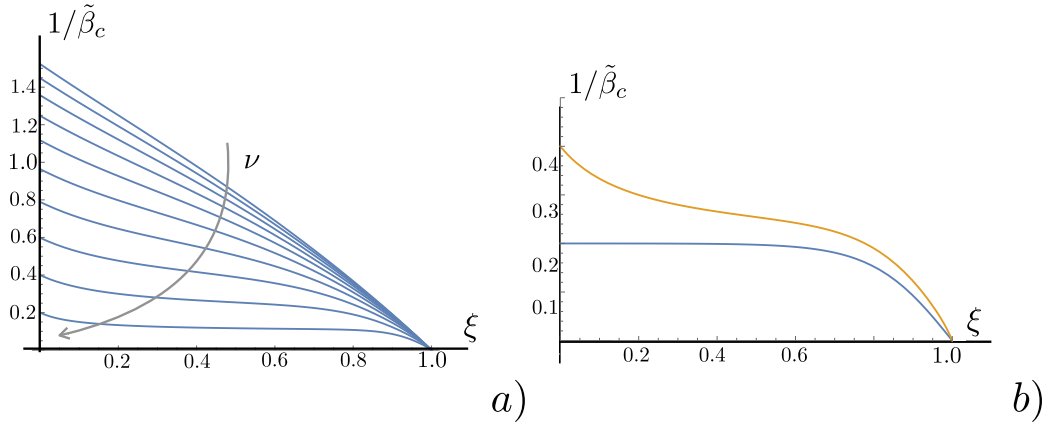

Fig. 14. (a): Behavior of the critical temperature ($\delta = 1$) as a function of the decohesion fraction ξ, at variable values of $\nu \in (0.1, 1)$. (b) Comparison of the effective critical temperatures $1/\tilde{\beta}^G_c(\xi)$ and $1/\tilde{\beta}^H_{c,1}(\xi)$ as a function of the decohesion fraction ξ. The Helmholtz ensemble corresponds to the yellow line ($\delta = 1$), and Gibbs one to the blue line. Here, we assumed $\nu = 0.2$.

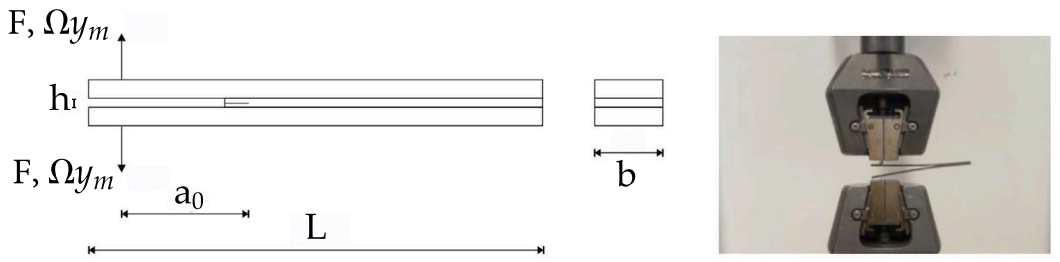

Fig. 15. Schematic representation of DCB test. Left panel: geometry of the DCB specimen. Right panel: photography of a DCB test. Adapted with permission from the literature (Fernandes et al., 2016).

with $T^H_{c,0}$ defined by Eq. (104), where $\delta = 0$. Otherwise, if we assume $\delta = 1$, we find that

$$\Omega_c(\xi, T) = \sqrt{1 + \left[(\Omega_c^o)^2 - 1\right]\left(1 - \frac{T}{T^H_{c,1}}\right)}. \tag{107}$$

with $T^H_{c,1}$ defined by Eq. (104), where $\delta = 1$.

This second choice is interesting because it eliminates some singularities present in the first one. We therefore use it in some illustrative graphs. The behavior of the threshold extension Ω_c, and the corresponding force Q_c, versus the effective temperature $1/\tilde{\beta}$ is shown in Fig. 12, for different values of the detached fraction ξ, see Eqs. (99) and (100).

Some examples of the analysis of the decohesion front propagation are presented in Fig. 13. In particular, Fig. 13*a* illustrates the critical displacement threshold Ω_c as a function of the initial detached fraction ξ, for different temperatures T. Specifically, we consider three distinct temperature regimes: curve A represents the mechanical system at $T = 0$, curve B corresponds to the case where $0 < T < T^H_{c,1}$, and curve C describes the scenario where $T > T^H_{c,1}$. Notably, curve C consistently represents a system undergoing spontaneous decohesion induced by thermal fluctuations. It is interesting to observe that the displacement thresholds decrease as the temperature increases. Additionally, among the three curves depicting the critical threshold as a function of detached portions, we focus on three particular values: $\xi_1 = 0$, which characterizes the nucleation behavior, $\xi_2 > \xi_1$, and $\xi_3 > \xi_2$. In Fig. 13 (panels *b*, *c*, and *d*), we present the force–displacement decohesion behavior for three systems corresponding to the three considered values of ξ. Each panel shows three curves (corresponding to the three previously mentioned temperature regimes) that describe the response of systems with different initial detached portions. Specifically, Fig. 13*b* highlights the nucleation behavior of the system ($\xi_1 = 0$). Panels *c* and *d* focus on systems with initial detachments ξ_2 and ξ_3, respectively. It is important to note that when the initial detached portion is ξ_3, the system exceeds the critical threshold even for the temperature of case *B*. Consequently, sudden full decohesion occurs as the temperature-dependent Griffith condition is met.

The behavior of $1/\tilde{\beta}^H_{c,1}$ can be found in Fig. 14*a*, where we showed the effective critical temperature versus ξ for different values of ν. We deduce that the critical temperature is low for ξ approaching 1 since the system is almost completely detached, and $T^H_{c,1}$ increases when ξ decreases.

It is interesting to note that the critical temperature in detached systems with hard and soft devices is different and that the system with assigned displacement is always more stable than the system with assigned force. In Fig. 14*b* we compare the two critical parameters $1/\tilde{\beta}^G_c(\xi)$ and $1/\tilde{\beta}^H_{c,1}(\xi)$.

To conclude, the resulting thermally activated detachment is explained by a cooperative process induced by the thermal fluctuations. This behavior exactly corresponds to a second order phase transition for which we defined the critical temperature in closed form. As already remarked for the Gibbs ensemble, it is important to reiterate that the critical temperature depends on the initial state of detachment of the system. This behavior comes from the fact that we perform a continuum limit and not a thermodynamic limit.

3.3. Comparison with experimental results

To evaluate the effectiveness of our proposed model in understanding detachment processes influenced by temperature, we compare our theoretical results with experiments on the decohesion behavior of carbon-epoxy composite bonded joints, conducted at different temperatures and reported by Fernandes et al. (2016). These experiments are prompted by the widespread use of bonded joints, as this bonding method provides a more uniform stress distribution on the bonded area, reduces stress concentrations, and offers high fatigue resistance, making it more efficient and flexible in design compared to other joining methods such as welding, bolting, and riveting. Due to these advantages, adhesive joints have a wide range of applications and are often exposed to extreme conditions, including high temperature regimes. Generally, the strength of bonded joints is affected by temperature, showing decreasing performances at very high or low temperatures (Ashcroft et al., 2001; Hu et al., 2013; Marques et al., 2015). In particular, temperature effects on bonded joints varies depending on the adopted type of adhesive and adherent used. However, the fracture toughness of bonded joints exposed to adverse environmental conditions has received relatively little attention from researchers.

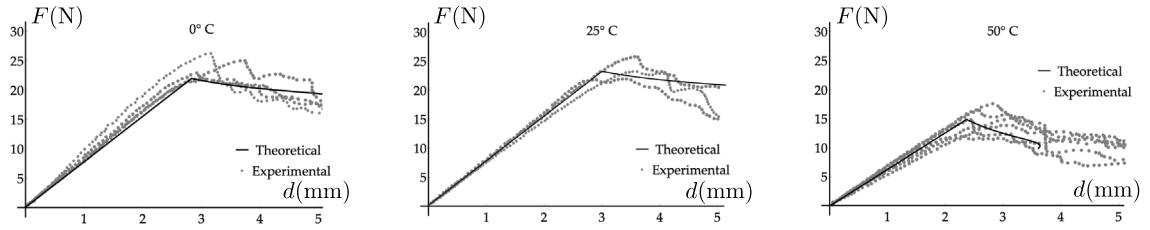

Fig. 16. Force–extension response describing the decohesion process of the double-cantilever beam. We compare the results obtained from the theoretical model with experimental data from the literature (Fernandes et al., 2016). The measured load F is represented in N and the applied displacement Ωy_m in mm.

Here we consider as prototypical example of the described thermal effects the experiments by Fernandes et al. (2016), where the authors study the effects of temperature on the decohesion of bonded joints made with carbon-epoxy laminate and structural adhesive, see Fig. 15. For the experiment, several double-cantilever-beam (DCB) specimens were prepared by extracting carbon-epoxy laminate from carbon-epoxy plates using SEAL® Texipreg HS 160 RM. The bonding to metallic hinges for DCB test was then performed at room temperature using a ductile epoxy adhesive, namely Araldite® 2015 with $E = 1850$ MPa and $\nu = 0.3$ (de Moura et al., 2009). The specimens were then exposed to two higher temperatures (0 °C and 50 °C) chosen as representative of the climatic conditions to which typical bonded joint structures can be exposed. The glass transition temperature of the adhesive is $T_g = 75 \pm 5$ °C, confirming that the higher temperature adopted (50 °C) is anyhow lower than the glass transition temperature of the adhesive. The authors discuss a set of load–displacement curves for each temperature of the tested specimens.

The aim of this section is then to verify the possibility of predicting the experimental behavior for the three different temperatures with our analytical model. It is important to note that our model could slightly underestimate the total energy of the experimental system (adherend, adhesive, and metallic hinges) because it only provides an estimation of the adhesive energy, neglecting, for example, the carbon-epoxy laminate deformation energy. This is accounted for by effective values of the constitutive parameters adopted in our model, which represent the equivalent real system. This means, for example, that the values used for elastic and shear moduli are equivalent parameters obtained by taking into account the deformation energy of both the adherent and the adhesive, and that the metal hinges are much stiffer than the adhesive.

A rescaling of the entropic contribution of the energy is also necessary because, to consider the temperature effects in a polymeric material such as the adhesive used, the entropic part of the energy must be rescaled by the number of polymer chains per unit volume (roughly 10^{27}) (Beatty, 2003; De Tommasi et al., 2015; Puglisi et al., 2017; Treloar, 1975). Specifically, regarding the entropic contribution, we also consider that the process zone described by our theoretical model corresponds to a given percentage of the total adhesive height. The geometry is described by a total length $L = 150$ mm, a depth $b = 3$ mm, a total height of the adhesive $h = 2$ mm, as shown in Fig. 15. In addition, before the DCB test, the samples were subjected to an initial de-adhesion of $a_0 = 40$ mm, created with a razor blade. This initial de-adhesion corresponds to a detached region of $\xi = 0.267$ for our model.

Elastic and shear moduli are fitted based on the first curve, with subsequent curves obtained assuming that the elastic modulus is approximately constant at 0 °C and 25 °C and decreases at higher temperatures. By applying Eqs. (6) and (75), we deduce $E = 111\,200$ Pa for the first two experiments and $E = 90\,610$ Pa for the third one. The shear modulus for all three cases is determined by considering a ratio of $\mu/E = 6500$, chosen in line with the fact that the adhesive is bonded to metallic hinges, which are much stiffer compared to the adhesive material. Then, using Eq. (99), we derive both the process region height for proper entropy rescaling (7% of total height h) and the fracture energy estimate $\frac{1}{2}Ey_m^2$, leading to $y_m = 1.25$ mm.

The comparison between theoretical and experimental results is shown in Fig. 16. Each panel displays the experimental data points for a given temperature, with the black curve representing the proposed theoretical load–displacement behavior. A good agreement between experimental data and theoretical model results is finally pointed out.

4. Conclusions and remarks

In this work, we have introduced a prototypical model showing the possibility of measuring the impact of thermal fluctuations into continuous models of adhesion/deadhesion processes. To facilitate the integration of Statistical Mechanics into this framework, we initially developed a discrete model with n elements, which we subsequently extended through the continuum limit. To achieve this, we defined the physical parameters of the system ensuring the appropriate rescaling as n approaches infinity.

Neglecting temperature effects, it is possible to directly ascertain the limit as n approaches infinity for the system's energy by eventually expressing it in integral form. This energy can subsequently be minimized using the classical energetic variational approach, akin to the application of Griffith's stability criterion of linear elastic fracture mechanics. This approach enables us to determine the threshold that must be exceeded by the purely mechanical action applied to induce the deadhesion of the system. Remarkably our model is able to determine, differently from the classical Griffith approach, also the nucleation phenomenon and the corresponding load thresholds. Moreover we are able to distinguish stable and unstable detachment propagation by differentiating between force-controlled and displacement-controlled experiments.

On the other hand, when considering temperature effects, it becomes necessary to compute the partition function by working with the discrete model, wherein the coordinates of each element can be clearly defined. We then determine the continuum limit

as n tends towards infinity, allowing for the calculation of the free energy. The free energy accounts for both mechanical energies and entropic contributions. It is important to emphasize that, in this context, the Griffith criterion relies on the use of free energy in place of total energy.

By following the Griffith's approach we adopted a phenomenological perspective in describing the complex phenomenon of energy dissipation. Specifically, we adopted a Statistical Mechanics approach considering a *constrained minimization problem* determining the expected values of the parameters by averaging on the free energy manifolds at fixed decohesion fraction ξ. The fracture evolution is then assigned phenomenologically by analyzing the driving force at the origin of the fracture front propagation according to the classical Griffith approach. We remark that this approach is the opposite of alternative methods used to describe fracture and decohesion phenomena, such as the global energy minimization proposed by Francfort and Marigo (1998), or explored by Florio et al. (2020).

It is also important to highlight that, in our approach, we minimized the free energy, considering the quantities $H - TS$ (Gibbs, with H the enthalpy and S the entropy) or $U - TS$ (Helmholtz, with U the internal energy), under the hypothesis of isothermal processes. All the complex dissipation phenomena are then accounted by considering the debonding energy of the breakable elements. Observe that an *ad hoc* irreversibility assumption can be introduced by requiring that, during the unloading phase, the debonded fraction cannot reattach. Nevertheless, of course, any real decohesion processes (at arbitrary rate) inherently involves entropy production for two fundamental reasons, *i.e.* dissipation and heat transfer generated during the process (these two phenomena are explicitly neglected in our theory but are implicitly accounted for in the fracture energy of each individual breakable link). Therefore, our approach may seem at odds with the second law of thermodynamics and entropy production, and one may ask why we can obtain meaningful results capable of interpreting experimental findings (at least in certain cases) without employing out-of-equilibrium Statistical Mechanics or, equivalently, the second law of thermodynamics. The answer lies in the time scale separation whose validity depends on the specific problem at study. In other words, the process depends on the rate at which the load (force or displacement), causing decohesion, is applied. To better explain this point, let us consider the discrete model: each successive breaking of a link in the adhesive corresponds to overcoming a small energy barrier, much like as in the process of a chemical reaction. Thus, each link rupture can be seen as a bistable element, described by two energy wells separated by an energy barrier (Buche & Grutzik, 2024; Persson, 2024). Such a system inherently has rate coefficients that describe the transitions between states as a function of the system's temperature (as per Kramers rate theory or transition state theories) (Bellino, 2022; Cannizzo & Giordano, 2024; Giordano et al., 2023; Hänggi et al., 1990; Kramers, 1940). Therefore, if the loading rate is very low, these rate coefficients allow the system to follow the evolution of the load, enabling near-instantaneous re-equilibration. This means that the quasi-spontaneous transitions between states automatically re-balance the system, causing the links to break without further macroscopic consequences. This scenario exactly describes the regime in which our model is valid, and it fortunately corresponds to numerous practical situations. In particular, this regime is coherent for systems exhibiting rate independent behavior. Naturally, to determine the actual limits of validity, one would need to compare the intrinsic rates with the loading rate, which is not a straightforward task. When the loading rate is high, the system does not have enough time to re-equilibrate and follow the changes imposed by the load. This regime is completely out of equilibrium, leading to a macroscopic response to this situation: typically, the force required to break the bonds increases significantly with the loading rate. In fact, the additional energy required is used to compensate for the re-equilibration, and this is effectively described by a higher entropy production.

As a final result of the modeling, we are able to analytically determine the decreasing of the decohesion threshold depending on temperature. Interestingly, this procedure leads to the identification of a phase transition, which characterizes the thermoactivated deadhesion at supercritical temperatures. This approach has been employed in two distinct statistical ensembles: the load-controlled Gibbs ensemble, which involves the application of force by a soft device to detach the film, and the displacement-controlled Helmholtz ensemble, where the position of one end of the film is specified by a hard device. The responses in these two statistical ensembles differ due to the distinct phase spaces imposed by the boundary conditions. It is evident that the Helmholtz conditions are more constraining as they prescribe the position of one end of the film, thereby reducing the influence of temperature-induced fluctuations. Interestingly, this distinction can be directly observed from the curves illustrating the variations in the effective critical temperature as the system parameters evolve. When considering the same initial detachment state, denoted as ξ, and the same elastic ratio, represented as ν, it becomes evident that the critical temperature is consistently higher for the Helmholtz ensemble as compared to the Gibbs ensemble. This contrast can be substantiated by observing Fig. 14 (panel *b*). This result underscores the reduced impact of thermal fluctuations in isometric continuous systems compared to isotensional ones. On the other hand coherent decohesion fronts propagation are obtained in the hard device, whereas the decohesion is always fragile in the soft device regime. These findings reveal significant and intriguing disparities in the critical behavior of continuous adhesion models across different statistical ensembles. In contrast to discrete models that have been extensively explored in prior literature, continuous models highlight a distinctive feature – the critical temperature's dependence on the initial attachment state of the film deposited on the substrate. This aspect warrants further investigation, particularly from an experimental perspective. It is worth noting that the existence of a phase transition in the deadhesion process, as described by continuous models, plays a pivotal role in the interpretation of numerous physical phenomena outlined broadly in the Introduction. For instance, an example of comparison between theory and recent experiments on bonded joints is discussed from a qualitative and quantitative point of view.

While the proposed models provide valuable insights into the critical behavior of adhesion processes, they stand to benefit from further refinement to encompass additional physical phenomena.

In the model considered, we accounted only for shear springs in both the discrete and subsequent continuous formulations. Naturally, this assumption can be overcome with more accurate models, as discussed in details in Section 2.1. The possibility of considering soft substrates could expand the applicability of the model not only to soft materials and biophysics but also to

mechanical engineering in cases where the film and substrate exhibit similar elastic responses. One of the simplest methods to develop this generalization is to introduce two rows of vertical (linear) springs into the system, assuming that the lower row represents the elasticity of the substrate (unbreakable), while the upper row represents the adhesive bond between the film and the substrate (breakable). Naturally, the model should be completed with shear (linear) springs that represent the film itself, as in our original model. The introduction of springs into the substrate changes the decohesion propagation thresholds according to Griffith's theory, both under force-controlled and displacement-controlled conditions. The effects of the soft substrate become even more significant when temperature is considered. Indeed, in this case, the entropic forces from the substrate can notably influence the decohesion process. This discrete approach can also be used to derive a continuum model, which can be formulated using variational principles and involves two displacement functions as unknowns, instead of just one. We would like to emphasize that this approach has already been implemented in the study of friction on a soft substrate (Giordano, 2023).

Another important extension is to consider a possible intermediate softening state of the adhesive (layer made of breakable springs) that is observed between the fully detached and fully attached states. This state may represent a more progressive weakening of the attached state useful, for example, in introducing the brittle-to-ductile transition of the material. This transition being handled by thermal effects, is studied perfectly by Statistical Mechanics (Cannizzo & Giordano, 2023; Kovács et al., 2013; Rice & Thomson, 1974).

As remarked above, we have overlooked dynamic processes as our approach relied on Statistical Mechanics in an equilibrium setting. To address non-equilibrium effects, it is possible to introduce dynamic considerations by formulating the Langevin and Fokker–Planck equations pertaining to the adhesion problem at hand, and subsequently seeking solutions through approximate analytical or numerical methods. Typical approximations are based on the transition state theory or the well-known Kramers formula for reaction kinetics (Bellino, 2022; Cannizzo & Giordano, 2024; Giordano et al., 2023; Hänggi et al., 1990; Kramers, 1940).

Finally, our analysis has consistently focused on homogeneous systems, whereas real-world systems often exhibit heterogeneity. The incorporation of disorder is a crucial aspect to consider since it can substantially impact the critical behavior of these systems (Borja da Rocha & Truskinovsky, 2022).

CRediT authorship contribution statement

Claudia Binetti: Software, Methodology, Data curation, Conceptualization. **Andrea Cannizzo:** Methodology, Formal analysis. **Giuseppe Florio:** Methodology, Investigation, Conceptualization. **Nicola M. Pugno:** Validation, Supervision, Investigation, Conceptualization. **Giuseppe Puglisi:** Writing – review & editing, Supervision, Methodology, Investigation, Data curation, Conceptualization. **Stefano Giordano:** Writing – original draft, Supervision, Methodology, Investigation, Formal analysis, Conceptualization.

Declaration of competing interest

The authors declare that they have no known competing financial interests or personal relationships that could have appeared to influence the work reported in this paper.

Acknowledgments

The authors have been supported by Central Lille and Region Hauts-de-France under project MIBAMS (Modeling micro Instabilities in Biophysics And Materials Science), and by Polytechnic of Bari, University of Trento, Italy and Region Hauts-de-France under project STAMENA (STAtistical MEchanics for macromolecular structures of NAnotechnology). C.B., G.F. and G.P. have been supported by GNFM - Gruppo Nazionale per la Fisica Matematica - INdAM. G.F and G.P.'s research is funded by the European Union - Next Generation EU. G.P and G.P. are supported by PNRR, National Center for HPC, Big Data and Quantum Computing - M4C2 - I 1.4 (grant number CN00000013, CUP D93C22000430001) - Spoke 5 (Environment and Natural Disasters). G.P. has been supported by the Project of National Relevance PRIN2022 (grant number 2022XLBLRX, CUP D53D23006020006) and PRIN2022PNRR (grant number P2022KHFNB, CUP D53D23018910001) granted by the Italian MUR. G.F. has been supported by the Project of National Relevance PRIN2022 (grant number 2022MKB7MM, CUP D53D2300590 0006) and PRIN2022PNRR (grant number P2022MXCJ2, CUP D53D23018940001) granted by the Italian MUR. G.F. is also supported by INFN project QUANTUM.

Appendix A. Determination of the asymptotic behavior of $\det \boldsymbol{B}_G$

Since the matrices $\boldsymbol{B}_G$ and $\boldsymbol{A}_G$ are tridiagonal, we can analytically evaluate their inverse and their determinant by standard techniques (Usmani, 1994a, 1994b). We consider a generic tridiagonal matrix $\boldsymbol{M}$, and we define its elements as $\boldsymbol{M}_{i,i} = b_i$ (main diagonal), $\boldsymbol{M}_{i,i-1} = a_i$ (lower diagonal), and $\boldsymbol{M}_{i,i+1} = c_i$ (upper diagonal). All other elements are zero. We can introduce the quantities θ_i by means of the following recurrence relation

$$\begin{cases} \theta_i = b_i\theta_{i-1} - a_i c_{i-1}\theta_{i-2}, \\ \theta_{-1} = 0,\ \theta_0 = 1,\ i = 1, 2, \dots, n, \end{cases} \tag{A.1}$$

where, in particular, $\theta_n = \det \boldsymbol{M}$. Furthermore, it is possible to define the quantities ϕ_i through the recurrence formula

$$\begin{cases} \phi_i = b_i\phi_{i+1} - c_i a_{i+1}\phi_{i+2}, \\ \phi_{n+2} = 0,\ \phi_{n+1} = 1,\ i = n, n-1, \dots, 1, \end{cases} \tag{A.2}$$

where $\phi_1 = \theta_n = \det \boldsymbol{M}$. These definitions can be used to determine the elements of the inverse matrix $\boldsymbol{M}^{-1}$ (Usmani, 1994a, 1994b), as follows

$$(\boldsymbol{M}^{-1})_{i,j} = \begin{cases} \dfrac{(-1)^{i+j} c_i c_{i+1} \dots c_{j-1} \theta_{i-1} \phi_{j+1}}{\theta_n}, & \text{if } i < j, \\ \dfrac{\theta_{i-1}\phi_{i+1}}{\theta_n}, & \text{if } i = j, \\ \dfrac{(-1)^{i+j} a_{j+1} a_{j+2} \dots a_i \theta_{j-1} \phi_{i+1}}{\theta_n}, & \text{if } i > j. \end{cases} \tag{A.3}$$

By considering our particular case, the elements in the main diagonal of $\boldsymbol{A}_G$ are defined as $a_i = 2 + \mu$ for $1 \le i \le p$, and $a_i = 2$ for $p + 1 \le i \le n$. We have $\mu = 1/(n^2\nu^2)$, in agreement with Eq. (35). Moreover, we have that $\boldsymbol{A}_{G\ i,i+1} = \boldsymbol{A}_{G\ i+1,i} = -1$ for the upper and lower diagonals. For this special situation, θ_i and ϕ_i are defined by the rules

$$\begin{cases} \theta_i = a_i \theta_{i-1} - \theta_{i-2}, \\ \theta_{-1} = 0,\ \theta_0 = 1,\ i = 1, 2, \dots, n, \end{cases} \tag{A.4}$$

and

$$\begin{cases} \phi_i = a_i \phi_{i+1} - \phi_{i+2}, \\ \phi_{n+2} = 0,\ \phi_{n+1} = 1,\ i = n, n-1, \dots, 1. \end{cases} \tag{A.5}$$

Consequently, the elements of the inverse matrix $\boldsymbol{A}_G^{-1}$ are given by

$$(\boldsymbol{A}_G^{-1})_{i,j} = \begin{cases} \dfrac{\theta_{i-1}\phi_{j+1}}{\theta_n}, & \text{if } i < j, \\ \dfrac{\theta_{i-1}\phi_{i+1}}{\theta_n}, & \text{if } i = j, \\ \dfrac{\theta_{j-1}\phi_{i+1}}{\theta_n}, & \text{if } i > j. \end{cases} \tag{A.6}$$

The solution of the difference equations stated in Eqs. and can be found by defining the function

$$\boldsymbol{G}(\gamma, z) = \frac{1}{\sqrt{\Delta_\gamma}} \left[\left(\frac{2 + \gamma + \sqrt{\Delta_\gamma}}{2} \right)^z - \left(\frac{2 + \gamma - \sqrt{\Delta_\gamma}}{2} \right)^z \right], \tag{A.7}$$

with $\Delta_\gamma = \gamma^2 + 4\gamma$. The final solution for θ_i, when $i \le p$, is

$$\theta_i = \boldsymbol{G}(\mu, i + 1). \tag{A.8}$$

Moreover, the solution for θ_i, when $i \ge p + 1$, reads

$$\theta_i = \boldsymbol{G}(\mu, p)(p - i) + \boldsymbol{G}(\mu, p + 1)(i - p + 1). \tag{A.9}$$

We obtain ϕ_i, for $i \ge p + 1$, in the form

$$\phi_i = n + 2 - i. \tag{A.10}$$

Finally, we find ϕ_i, when $i \le p$, as follows

$$\phi_i = (n - p)\boldsymbol{G}(\mu, i - p - 1) - (n - p + 1)\boldsymbol{G}(\mu, i - p - 2). \tag{A.11}$$

The obtained values of θ_i and ϕ_i allow the calculation of $\boldsymbol{A}_G^{-1}$ and $\det \boldsymbol{A}_G$. From Eq. (34), we can write

$$\det \boldsymbol{B}_G = (n^2\nu^2)^n \det \left(\boldsymbol{A}_G - \boldsymbol{e}_1 \otimes \boldsymbol{e}_1 - \boldsymbol{e}_n \otimes \boldsymbol{e}_n \right). \tag{A.12}$$

We introduce now the following two properties. We consider a matrix $\boldsymbol{C}$ and a vector $\boldsymbol{c}$ such that $\boldsymbol{C}^{-1}$ and $(\boldsymbol{C} + x\boldsymbol{c} \otimes \boldsymbol{c})^{-1}$ exist for some real x. Under these assumptions, the two following relations can be proved (Giordano, 2023)

$$(\boldsymbol{C} + x\boldsymbol{c} \otimes \boldsymbol{c})^{-1} = \boldsymbol{C}^{-1} - x \frac{\boldsymbol{C}^{-1}\boldsymbol{c} \otimes \boldsymbol{c}\boldsymbol{C}^{-1}}{1 + x\boldsymbol{c} \cdot \boldsymbol{C}^{-1}\boldsymbol{c}}, \tag{A.13}$$

$$\det (\boldsymbol{C} + x\boldsymbol{c} \otimes \boldsymbol{c}) = \det \boldsymbol{C} \left(1 + x\boldsymbol{c} \cdot \boldsymbol{C}^{-1}\boldsymbol{c} \right). \tag{A.14}$$

By using these relations, Eq. (A.12) can be rewritten as

$$\det \boldsymbol{B}_G = (n^2\nu^2)^n \det\left(\boldsymbol{A}_G\right)\left[\left(1-(\boldsymbol{A}_G^{-1})_{11}\right)\left(1-(\boldsymbol{A}_G^{-1})_{nn}\right)-(\boldsymbol{A}_G^{-1})_{1n}^2\right], \tag{A.15}$$

where

$$\det\left(\boldsymbol{A}_G\right) = \theta_n = \boldsymbol{G}(\mu,p)(p-n)+\boldsymbol{G}(\mu,p+1)(n-p+1), \tag{A.16}$$

$$(\boldsymbol{A}_G^{-1})_{11} = \frac{\theta_0\phi_2}{\theta_n} = \frac{\boldsymbol{G}(\mu,1-p)(n-p)-\boldsymbol{G}(\mu,-p)(n-p+1)}{\boldsymbol{G}(\mu,p)(p-n)+\boldsymbol{G}(\mu,p+1)(n-p+1)}, \tag{A.17}$$

$$(\boldsymbol{A}_G^{-1})_{nn} = \frac{\theta_{n-1}\phi_{n+1}}{\theta_n} = \frac{\boldsymbol{G}(\mu,p)(p-n+1)+\boldsymbol{G}(\mu,p+1)(n-p)}{\boldsymbol{G}(\mu,p)(p-n)+\boldsymbol{G}(\mu,p+1)(n-p+1)}, \tag{A.18}$$

$$(\boldsymbol{A}_G^{-1})_{1n} = \frac{\theta_0\phi_{n+1}}{\theta_n} = \frac{1}{\boldsymbol{G}(\mu,p)(p-n)+\boldsymbol{G}(\mu,p+1)(n-p+1)}. \tag{A.19}$$

For the last three expressions, we took advantage of Eq. (A.6), where we substituted the solutions for θ_i and ϕ_i. Then, by using the definition of the function $\boldsymbol{G}$ defined in Eq. (A.7), we obtain the following asymptotic behaviors

$$\det \boldsymbol{A}_G \underset{n\to\infty}{\sim} n\left[\nu\sinh\left(\frac{1-\xi}{\nu}\right)+\xi\cosh\left(\frac{1-\xi}{\nu}\right)\right], \tag{A.20}$$

$$1-(\boldsymbol{A}_G^{-1})_{11} \underset{n\to\infty}{\sim} \frac{\xi\sinh\left(\frac{1-\xi}{\nu}\right)+\nu\cosh\left(\frac{1-\xi}{\nu}\right)}{n\nu\left[\nu\sinh\left(\frac{1-\xi}{\nu}\right)+\xi\cosh\left(\frac{1-\xi}{\nu}\right)\right]}, \tag{A.21}$$

$$1-(\boldsymbol{A}_G^{-1})_{nn} \underset{n\to\infty}{\sim} \frac{\cosh\left(\frac{1-\xi}{\nu}\right)}{n\left[\nu\sinh\left(\frac{1-\xi}{\nu}\right)+\xi\cosh\left(\frac{1-\xi}{\nu}\right)\right]}, \tag{A.22}$$

$$(\boldsymbol{A}_G^{-1})_{1n} \underset{n\to\infty}{\sim} \frac{1}{n\left[\nu\sinh\left(\frac{1-\xi}{\nu}\right)+\xi\cosh\left(\frac{1-\xi}{\nu}\right)\right]}. \tag{A.23}$$

To conclude, by substituting these results in Eq. (A.15) for $\det \boldsymbol{B}_G$, we obtain Eq. (49) of the main text. This methodology, although with a longer procedure, can be also applied to demonstrate the $\Gamma-$convergence of the Gibbs energy functional. For the sake of brevity, we do not report all the details here.

Appendix B. Determination of the asymptotic behavior of $\det \boldsymbol{B}_H$

To obtain the asymptotic behavior of $\det \boldsymbol{B}_H$, we use several results of previous Appendix A. To begin, from Eq. (83), we obtain

$$\det \boldsymbol{B}_H = (n^2\nu^2)^{n-1}\det(\boldsymbol{A}_H - \boldsymbol{e}_1\otimes\boldsymbol{e}_1), \tag{B.1}$$

where we utilize Eq. (A.14) to get

$$\det \boldsymbol{B}_H = (n^2\nu^2)^{n-1}\det(\boldsymbol{A}_H)\left(1-(\boldsymbol{A}_H^{-1})_{11}\right). \tag{B.2}$$

Now, from previous analysis, we have that

$$\det \boldsymbol{A}_H \underset{n\to\infty}{\sim} n\left[\nu\sinh\left(\frac{1-\xi}{\nu}\right)+\xi\cosh\left(\frac{1-\xi}{\nu}\right)\right], \tag{B.3}$$

$$1-(\boldsymbol{A}_H^{-1})_{11} \underset{n\to\infty}{\sim} \frac{\xi\sinh\left(\frac{1-\xi}{\nu}\right)+\nu\cosh\left(\frac{1-\xi}{\nu}\right)}{n\nu\left[\nu\sinh\left(\frac{1-\xi}{\nu}\right)+\xi\cosh\left(\frac{1-\xi}{\nu}\right)\right]}. \tag{B.4}$$

To conclude, we can substitute these expressions in Eq. (B.2) to obtain Eq. (93) of the main text. As before, this approach is also useful for proving the $\Gamma-$convergence within the Helmholtz ensemble.

Data availability

No data was used for the research described in the article.

References

Adams, R. D., Coppendale, J., Mallick, V., & Al-Hamdan, H. (1992). The effect of temperature on the strength of adhesive joints. *International Journal of Adhesion and Adhesives*, *12*, 185–190.

Anderson, T. L. (2005). *Fracture mechanics: fundamentals and applications*. Boca Raton: CRC Press.

Ashcroft, I. A., Hughes, D. J., & Shaw, S. J. (2001). Mode I fracture of epoxy bonded composite joints: 1. Quasi-static loading. *International Journal of Adhesion and Adhesives*, *21*, 87–99.

Awada, H., Hamieh, O., Kazzi, Y., & Brogly, M. (2011). Contributions of chemical and mechanical surface properties and temperature effect on the adhesion at the nanoscale. *Thin Solid Films*, *519*, 3690–3694.

Baldan, A. (2012). Adhesion phenomena in bonded joints. *International Journal of Adhesion & Adhesives*, *38*, 95–116.

Barker, R. E. (1963). An approximate relation between elastic moduli and thermal expansivities. *Journal of Applied Physics*, *34*, 107–116.

Barreau, V., Yu, D., Hensel, R., & Arzt, E. (2017). Elevated temperature adhesion of bioinspired polymeric micropatterns to glass. *Journal of the Mechanical Behavior of Biomedical Materials*, *76*, 110–118.

Bayer, P. D., & Cooper, R. E. (1969). The tensile strength of sapphire whiskers at elevated temperatures. *Journal of Materials Science*, *4*, 15–20.

Beatty, M. F. (2003). An average-stretch full-network model for rubber elasticity. *Journal of Elasticity*, *70*, 65–86.

Bellino, L. (2022). *Temperature and rate effects in damage and decohesion of biological materials* (Ph.D. thesis), University of Bari, arXiv:2210.14193.

Bellino, L., Florio, G., Giordano, S., & Puglisi, G. (2020). On the competition between interface energy and temperature in phase transition phenomena. *Applications in Engineering Science*, *2*, Article 100009.

Bellino, L., Florio, G., Goriely, A., & Puglisi, G. (2023). Cooperative melting in double-stranded peptide chains through local mechanical interactions. *Journal of the Royal Society Interface*, *20*, Article 20230130.

Bellino, L., Florio, G., & Puglisi, G. (2019). The influence of device handles in single-molecule experiments. *Soft Matter*, *15*, 8680.

Benedito, M., & Giordano, S. (2018). Isotensional and isometric force-extension response of chains with bistable units and Ising interactions. *Physical Review E*, *98*, Article 052146.

Benedito, M., & Giordano, S. (2018). Thermodynamics of small systems with conformational transitions: The case of two-state freely jointed chains with extensible units. *Journal of Chemical Physics*, *149*, Article 054901.

Bihr, T., Seifert, U., & Smith, A.-S. (2012). Nucleation of ligand-receptor domains in membrane adhesion. *Physical Review Letters*, *109*, Article 258101.

Blom, K., & Godec, A. (2021). Criticality in cell adhesion. *Physical Review X*, *11*, Article 031067.

Borja da Rocha, H., & Truskinovsky, L. (2022). Mean field fracture in disordered solids: Statistics of fluctuations. *Journal of the Mechanics and Physics of Solids*, *158*, Article 104646.

Braides, A. (2002). *Γ-convergence for beginners*. Oxford University Press.

Brenner, S. S. (1962). Mechanical behavior of sapphire whiskers at elevated temperatures. *Journal of Applied Physics*, *33*, 33–39.

Bruin, C., & Compagner, A. (1973). A linear lattice gas with variable mesh size subject to gravity. *Physica*, *68*, 171–179.

Buche, M. R., & Grutzik, S. J. (2024). Statistical mechanical model for crack growth. *Physical Review E*, *109*, Article 015001.

Cannizzo, A., Bellino, L., Florio, G., Puglisi, G., & Giordano, S. (2022). Thermal control of nucleation and propagation transition stresses in discrete lattices with non-local interactions and non-convex energy. *European Physical Journal Plus*, *137*, 569.

Cannizzo, A., Florio, G., Puglisi, G., & Giordano, S. (2021). Temperature controlled decohesion regimes of an elastic chain adhering to a fixed substrate by softening and breakable bonds. *Journal of Physics A: Mathematical and Theoretical*, *54*, Article 445001.

Cannizzo, A., & Giordano, S. (2023). Thermal effects on fracture and the brittle-to-ductile transition. *Physical Review E*, *107*, Article 035001.

Cannizzo, A., & Giordano, S. (2024). Statistical mechanics approaches for studying temperature and rate effects in multistable systems. *Symmetry*, *16*, 632.

Cassidy, P. E., Johnson, J. M., & Locke, C. E. (1972). The relationship of glass transition temperature to adhesive strength. *Journal of Adhesion*, *4*, 183–191.

Chaudhury, M. K. (1999). Rate-dependent fracture at adhesive interface. *The Journal of Physical Chemistry B*, *103*, 6562–6566.

Chauhan, K., Mishra, G., Kishore, V., & Kumar, S. (2023). Appearance of de Gennes length in force-induced transitions. *Physical Review E*, *108*, L042501.

Ciavarella, M., Joe, J., Papangelo, A., & Barber, J. R. (2019). The role of adhesion in contact mechanics. *Journal of the Royal Society Interface*, *16*, Article 20180738.

Compagner, A. (1989). Thermodynamics as the continuum limit of statistical mechanics. *American Journal of Physics*, *57*, 106.

Creton, C., & Ciccotti, M. (2016). Fracture and adhesion of soft materials: a review. *Reports on Progress in Physics*, *79*, Article 046601.

Dasanna, A. K., Gompper, G., & Fedosov, D. A. (2020). Stability of heterogeneous parallel-bond adhesion clusters under load. *Physical Review Research*, *2*, Article 043063.

de Gennes, P.-G. (2001). Maximum pull out force on DNA hybrids. In *Série IV*: *Comptes Rendus de l'Académie des Sciences*, In *Série IV*: *2*.1505–1508,

De Lorenzo, S., Ribezzi-Crivellari, M., Arias-Gonzalez, J. R., Smith, S. B., & Ritort, F. (2015). A temperature-jump optical trap for single-molecule manipulation. *Biophysical Journal*, *108*, 2854–2864.

de Moura, M. F. S. F., Campilho, R. D. S. G., & Gonçalves, J. P. M. (2009). Pure mode II fracture characterization of composite bonded joints. *International Journal of Solids and Structures*, *46*, 1589–1595.

De Tommasi, D., Puglisi, G., & Saccomandi, G. (2015). Multiscale mechanics of macromolecular materials with unfolding domains. *Journal of the Mechanics and Physics of Solids*, *78*, 154–172.

Di Stefano, S., Florio, G., Napoli, G., Pugno, N., & Puglisi, G. (2022). On the role of elasticity in focal adhesion stability within the passive regime. *International Journal of Non-Linear Mechanics*, *146*, Article 104157.

Dillard, D. A., & Pocius, A. V. (2002). *The mechanics of adhesion*. Amsterdam, The Netherlands: Elsevier Science.

DiMilla, P. A., Barbee, K., & Lauffenburger, D. A. (1991). Mathematical model for the effects of adhesion and mechanics on cell migration speed. *Biophysical Journal*, *60*, 15–37.

Eick, J. D., Gwinnett, A. J., Pashley, D. H., & Robinson, S. J. (1997). Current concepts on adhesion to dentin. *Critical Reviews in Oral Biology & Medicine*, *8*, 306–335.

Fernandes, R., de Moura, M. F. S. F., & Moreira, R. D. F. (2016). Effect of temperature on pure modes I and II fracture behavior of composite bonded joints. *Composites Part B (Engineering)*, *96*, 35–44.

Florio, G., & Puglisi, G. (2019). Unveiling the influence of device stiffness in single macromolecule unfolding. *Scientific Reports*, *9*, 4997.

Florio, G., & Puglisi, G. (2023). A predictive model for the thermomechanical melting transition of double stranded DNA. *Acta Biomaterialia*, *157*, 225–235.

Florio, G., Puglisi, G., & Giordano, S. (2020). Role of temperature in the decohesion of an elastic chain tethered to a substrate by onsite breakable links. *Physical Review Research*, *2*, Article 033227.

Francfort, G. A., & Marigo, J. J. (1998). Revisiting brittle fracture as an energy minimization problem. *Journal of the Mechanics and Physics of Solids*, *46*, 1319–1342.

Fuhrmann, A., & Engler, A. J. (2015). The cytoskeleton regulates cell attachment strength. *Biophysical Journal*, *109*, 57–65.

Ghatak, A., Vorvolakos, K., She, H., Malotky, D. L., & Chaudhury, M. K. (2000). Interfacial rate processes in adhesion and friction. *The Journal of Physical Chemistry B*, *104*, 4018–4030.

Gibbs, J. W. (1902). *Elementary principles in statistical mechanics*. New York: Charles Scribner's Sons.

Giordano, S. (2017). Spin variable approach for the statistical mechanics of folding and unfolding chains. *Soft Matter*, *13*, 6877–6893.
Giordano, S. (2022). Statistical mechanics of rate-independent stick-slip on a corrugated surface composed of parabolic wells. *Continuum Mechanics and Thermodynamics*, *34*, 1343–1372.
Giordano, S. (2023). Temperature dependent model for the quasistatic stick–slip process on a soft substrate. *Soft Matter*, *19*, 1813.
Giordano, S., Cleri, F., & Blossey, R. (2023). On the one-dimensional transition state theory and the relation between statistical and deterministic oscillation frequencies of anharmonic energy wells. *Annals of Physics (Berlin)*, *2023*, Article 2300294.
Gojzewski, H., Kappl, M., & Ptak, A. (2017). Effect of the chain length and temperature on the adhesive properties of alkanethiol self-assembled monolayers. *Langmuir*, *33*, 11862–11868.
Goldenfeld, N. (2018). *Lectures on phase transitions and the renormalization group*. CRC-Press.
Gong, L., Xiang, L., Zhang, J., Chen, J., & Zeng, H. (2019). Fundamentals and advances in the adhesion of polymer surfaces and thin films. *Langmuir*, *35*, 15914–15936.
Griffith, A. A. (1921). The phenomena of rupture and flow in solids. *Philosophical Transactions of the Royal Society, Series A*, *221*, 163.
Gruhn, T., & Lipowsky, R. (2005). Temperature dependence of vesicle adhesion. *Physical Review E*, *71*, Article 011903.
Haisma, J., & Spierings, G. A. C. M. (2002). Contact bonding, including direct-bonding in a historical and recent context of materials science and technology, physics and chemistry - Historical review in a broader scope and comparative outlook. *Materials Science and Engineering Reports*, *37*, 1–60.
Hänggi, P., Talkner, P., & Borkovec, M. (1990). Reaction-rate theory: Fifty years after Kramers. *Reviews of Modern Physics*, *62*, 251–341.
Hu, P., X. Han, L. F. M. d. S., & Li, W. D. (2013). Strength prediction of adhesively bonded joints under cyclic thermal loading using a cohesive zone model. *International Journal of Adhesion and Adhesives*, *41*, 6–15.
Huang, K. (1987). *Statistical mechanics*. John Wiley & Sons.
Hyeon, C., & Thirumalai, D. (2005). Mechanical unfolding of RNA hairpins. *Proceedings of the National Academy of Sciences*, *102*, 6789–6794.
Israelachvili, J. N. (2011). *Intermolecular and surface forces*. Amsterdam, The Netherlands: Elsevier Science.
Itzykson, C., & Drouffe, J.-M. (1989). *Statistical field theory, volume 1: from Brownian motion to renormalization and lattice gauge theory*. Cambridge University Press.
Itzykson, C., & Drouffe, J.-M. (1989). *Statistical field theory, volume 2: strong coupling, Monte Carlo methods, conformal field theory and random systems*. Cambridge University Press.
Johnson, K. L. (1998). Mechanics of adhesion. *Tribology International*, *31*, 413–418.
Kendall, K. (1994). Adhesion: Molecules and mechanics. *Science*, *263*, 1720–1725.
Kendall, K. (2004). *Molecular adhesion and its applications - the sticky universe*. New York: Kluwer Academic Publishers.
Khalili, A. A., & Ahmad, M. R. (2015). A review of cell adhesion studies for biomedical and biological applications. *International Journal of Molecular Sciences*, *16*, 18149–18184.
Kim, H., Witt, H., Oswald, T. A., & Tarantola, M. (2020). Adhesion of epithelial cells to PNIPAm treated surfaces for temperature-controlled cell-sheet harvesting. *ACS Applied Materials & Interfaces*, *12*, 33516–33529.
Kleinert, H. (1990). *Path integrals in quantum mechanics, statistics and polymer physics*. London: World Scientific.
Kovács, K., Hidalgo, R. C., Pagonabarraga, I., & Kun, F. (2013). Brittle-to-ductile transition in a fiber bundle with strong heterogeneity. *Physical Review E*, *87*, Article 042816.
Kramers, H. A. (1940). Brownian motion in a field of force and the diffusion model of chemical reactions. *Physica*, *7*, 284–304.
Kwak, M. J., Kim, D. H., You, J. B., Moon, H., Joo, M., Lee, E., & Im, S. G. (2018). A sub-minute curable nanoadhesive with high transparency, strong adhesion, and excellent flexibility. *Macromolecules*, *51*, 992–1001.
Lai, T., Chen, R., & Huang, P. (2015). Temperature dependence of microscale adhesion force between solid surfaces using an AFM. *Journal of Adhesion Science and Technology*, *29*, 133–148.
Lake, G. J., & Thomas, A. G. (1967). The strength of highly elastic materials. *Proceedings of the Royal Society A*, *300*, 108–119.
Maddalena, F., Percivale, D., Puglisi, G., & Truskinovsky, L. (2009). Mechanics of reversible unzipping. *Continuum Mechanics and Thermodynamics*, *21*, 251.
Manca, F., Giordano, S., Palla, P. L., Zucca, R., Cleri, F., & Colombo, L. (2012). Elasticity of flexible and semiflexible polymers with extensible bonds in the Gibbs and Helmholtz ensembles. *Journal of Chemical Physics*, *136*, Article 154906.
Marques, E. A. S., da Silva, L. F. M., Banea, M. D., & Carbas, R. J. C. (2015). Adhesive joints for low- and high-temperature use: An overview. *Journal of Adhesion*, *91*, 556–585.
Marshall, S. J., Bayne, S. C., Baier, R., Tomsia, A. P., & Marshall, G. W. (2010). A review of adhesion science. *Dental Materials*, *26*, e11–e16.
Maso, G. D. (1993). *An introduction to Γ-convergence*. Birkhäuser.
Merkel, R., Nassoy, P., Leung, A., Ritchie, K., & Evans, E. (1999). Energy landscapes of receptor-ligand bonds explored with dynamic force spectroscopy. *Nature*, *397*, 50–53.
Miehe, C., Hofacker, M., & Welschinger, F. (2010). A phase field model for rate-independent crack propagation: Robust algorithmic implementation based on operator splits. *Computer Methods in Applied Mechanics and Engineering*, *199*, 2765.
Miracle, D. B., & Senkov, O. N. (2017). A critical review of high entropy alloys and related concepts. *Acta Materialia*, *122*, 448–511.
Mishra, G., Giri, D., Li, M. S., & Kumar, S. (2011). Role of loop entropy in the force induced melting of DNA hairpin. *Journal of Chemical Physics*, *135*, Article 035102.
Mishra, R. K., Modi, T., Giri, D., & Kumar, S. (2015). On the rupture of DNA molecule. *Journal of Chemical Physics*, *142*, Article 174910.
Mosayebi, M., Louis, A. A., Doye, J. P. K., & Ouldridge, T. E. (2015). Force-induced rupture of a DNA duplex: From fundamentals to force sensors. *ACS Nano*, *9*, 11993–12003.
Niewiarowski, P. H., Lopez, S., Ge, L., Hagan, E., & Dhinojwala, A. (2008). Sticky gecko feet: The role of temperature and humidity. *PLoS ONE*, *3*, Article e2192.
Parisi, G. (1988). *Statistical field theory*. Addison-Wesley Publishing Company, Inc..
Persson, B. N. J. (2024). Influence of temperature and crack-tip speed on crack propagation in elastic solids. *Journal of Chemical Physics*, *161*, Article 184704.
Peyrard, M. (2004). Nonlinear dynamics and statistical physics of DNA. *Nonlinearity*, *17*, R1–R40.
Peyrard, M., & Bishop, A. R. (1989). Statistical mechanics of a nonlinear model for DNA denaturation. *Physical Review Letters*, *62*, 2755–2758.
Pinon, A. V., Wierez-Kien, M., Craciun, A. D., Beyer, N., Gallani, J. L., & Rastei, M. V. (2016). Thermal effects on van der Waals adhesive forces. *Physical Review B*, *93*, Article 035424.
Puglisi, G., De Tommasi, D., Pantano, M. F., Pugno, N. M., & Saccomandi, G. (2017). Micromechanical model for protein materials: From macromolecules to macroscopic fibers. *Physical Review E*, *96*, Article 042407.
Puglisi, G., & Truskinovky, L. (2005). Thermodynamics of rate-independent plasticity. *Journal of the Mechanics and Physics of Solids*, *53*, 655–679.
Puglisi, G., & Truskinovsky, L. (2013). Cohesion-decohesion asymmetry in geckos. *Physical Review E*, *87*, Article 032714.
Pugno, N. M. (2021). The centenary of Griffith's theory. *Matter*, *4*, 3811.
Reister-Gottfried, E., Sengupta, K., Lorz, B., Sackmann, E., Seifert, U., & Smith, A.-S. (2008). Dynamics of specific vesicle-substrate adhesion: From local events to global dynamics. *Physical Review Letters*, *101*, Article 208103.
Ren, H. L., Zhuang, X. Y., Anitescu, C., & Rabczuk, T. (2019). An explicit phase field method for brittle dynamic fracture. *Computers and Structures*, *217*, 45.
Rice, J. R., & Thomson, R. (1974). Ductile versus brittle behaviour of crystals. *Philosophical Magazine*, *29*, 73.
Rico, F., Chu, C., Abdulreda, M. H., Qin, Y., & Moy, V. T. (2010). Temperature modulation of integrin-mediated cell adhesion. *Biophysical Journal*, *99*, 1387–1396.
Ron, J. E., Monzo, P., Gauthier, N. C., Voituriez, R., & Gov, N. S. (2020). One-dimensional cell motility patterns. *Physical Review Research*, *2*, Article 033237.

Schwarz, U. S., & Safran, S. A. (2013). Physics of adherent cells. *Reviews of Modern Physics*, *85*, 1327–1381.
Shao, J., Li, W., Li, Y., Deng, Y., Zhang, X., Kou, H., Xu, N., Zhang, X., Ma, J., Chen, L., & Qu, Z. (2019). Temperature-dependent fracture strength of whisker-reinforced ceramic composites: Modeling and factor analysis. *Journal of the American Ceramic Society*, *102*, 2841–2852.
Shull, K. R. (2002). Contact mechanics and the adhesion of soft solids. *Materials Science and Engineering Reports*, *36*, 1–45.
Singh, A., Modi, T., & Singh, N. (2016). Opening of DNA chain due to force applied on different locations. *Physical Review E*, *94*, Article 032410.
Speck, T., Reister, E., & Seifert, U. (2010). Specific adhesion of membranes: Mapping to an effective bond lattice gas. *Physical Review E*, *82*, Article 021923.
Stephenson, W., Keller, S., Santiago, R., Albrecht, J. E., Asare-Okai, P. N., Tenenbaum, S. A., Zuker, M., & Li, P. T. X. (2014). Combining temperature and force to study folding of an RNA hairpin. *Physical Chemistry Chemical Physics*, *16*, 906–917.
Stevens, R. N., & Guiu, F. (1991). Energy balance concepts in the physics of fracture. *Proceedings of the Royal Society of London. Series A*, *435*, 169–183.
Tang, T., Jagota, A., Chaudhury, M. K., & Hui, C.-Y. (2006). Thermal fluctuations limit the adhesive strength of compliant solids. *Journal of Adhesion*, *82*, 671–696.
Treloar, L. R. G. (1975). *The physics of rubber elasticity*. Oxford: Oxford University Press.
Usmani, R. A. (1994). Inversion of a tridiagonal Jacobi matrix. *Linear Algebra and its Applications*, *212–213*, 413.
Usmani, R. A. (1994). Inversion of Jacobi's tridiagonal matrix. *Computers & Mathematics with Applications*, *27*, 59.
Weiner, J. H. (1983). *Statistical mechanics of elasticity*. New York: Dover Publications.
Zehnder, A. T. (2012). *vol. 62*, *Fracture mechanics*. London: Lecture Notes in Applied and Computational Mechanics, Springer Science & Business Media.
Zhang, J., Das, S., & Du, Q. (2009). A phase field model for vesicle–substrate adhesion. *Journal of Computational Physics*, *228*, 7837–7849.
Zilberman, S., & Persson, B. N. J. (2003). Nanoadhesion of elastic bodies: Roughness and temperature effects. *Journal of Chemical Physics*, *118*, 6473–6480.
Zuckerman, D., & Bruinsma, R. (1995). Statistical mechanics of membrane adhesion by reversible molecular bonds. *Physical Review Letters*, *74*, 3900–3903.